

Input and output organization of the mesodiencephalic junction for cerebro-cerebellar communication

Xiaolu Wang¹ | Manuele Novello¹ | Zhenyu Gao¹ | Tom J. H. Ruigrok¹ |
Chris I. De Zeeuw^{1,2}

¹Department of Neuroscience, Erasmus MC, Rotterdam, the Netherlands

²Netherlands Institute for Neuroscience, Royal Dutch Academy of Arts & Science, Amsterdam, the Netherlands

Correspondence

Xiaolu Wang, Tom J. H. Ruigrok, and Chris I. De Zeeuw, Department of Neuroscience, Erasmus MC, 3000 CA Rotterdam, the Netherlands.

Email: x.wang@erasmusmc.nl (X. W.), t.ruigrok@erasmusmc.nl (T. J. H. R.), c.dezeeuw@erasmusmc.nl (C. I. D. Z.)

Funding information

This work was supported by ERC advanced, ZonMw, NWO-ALW, Medical NeuroDelta, INTENSE (LSH-NWO), Vriendenfonds Albinisme, and BIG (C.I.D.Z.); EUR fellowship, Erasmus MC fellowship, NWO VIDI, NWO-Klein, and ERC-stg grants (Z.G.)

Abstract

Most studies investigating the impact of the cerebral cortex (CC) onto the cerebellum highlight the role of the pons, which provides the mossy fibers to the cerebellum. However, cerebro-cerebellar communication may also be mediated by the nuclei of the mesodiencephalic junction (MDJ) that project to the inferior olive (IO), which in turn provides the climbing fibers to the molecular layer. Here, we uncover the precise topographic relations of the inputs and outputs of the MDJ using multiple, classical, and transneuronal tracing methods as well as analyses of mesoscale cortical injections from Allen Mouse Brain. We show that the caudal parts of the CC predominantly project to the principal olive via the rostral MDJ and that the rostral parts of the CC predominantly project to the rostral medial accessory olive via the caudal MDJ. Moreover, using triple viral tracing technology, we show that the cerebellar nuclei directly innervate the neurons in the MDJ that receive input from CC and project to the IO. By unraveling these topographic and prominent, mono- and disynaptic projections through the MDJ, this work establishes that cerebro-cerebellar communication is not only mediated by the pontine mossy fiber system, but also by the climbing fiber system.

KEYWORDS

cerebellar nuclei, cerebral cortex, climbing fiber, inferior olive, mesodiencephalic junction (MDJ), RRID:SCR_001622, RRID:SCR_002798

1 | INTRODUCTION

Cerebro-cerebellar communication can facilitate various forms of sensorimotor control (Akkal et al., 2007; Brown & Raman, 2018; Hamada et al., 2012; Popa et al., 2013; Proville et al., 2014; Quartarone et al., 2020) and cognitive processing (Brissenden & Somers, 2019; Crippa et al., 2016; Depping et al., 2018; D'Mello & Stoodley, 2015; Gao et al., 2018; Igelström et al., 2017; Olivito

et al., 2017). For example, it is required for active exploration during online coordination (Lindeman et al., 2021; Onuki et al., 2015), as well as for motor planning, and action perception during social cognition (Abdelgabar et al., 2019; Chabrol et al., 2019; Gao et al., 2018). Cerebro-cerebellar communication is organized in multiple reciprocal loops. The information route from the cerebellum to the cerebral cortex (CC) includes either a direct connection from the cerebellar nuclei (CN) onto various subnuclei of the thalamus (Amino et al., 2001;

Edited by Junie Paula Warrington and Scott T. Brady. Reviewed by Izumi Sugihara and Yosef Yarom.

Xiaolu Wang and Manuele Novello contributed equally to this work.

This is an open access article under the terms of the Creative Commons Attribution-NonCommercial License, which permits use, distribution and reproduction in any medium, provided the original work is properly cited and is not used for commercial purposes.

© 2021 The Authors. *Journal of Neuroscience Research* published by Wiley Periodicals LLC

Rispal-Padel & Grangetto, 1977; Shinoda et al., 1993), and/or a more indirect connection from the CN to prethalamic hubs like the zona incerta (Mitrofanis & deFonseka, 2001; Teune et al., 2000). Instead, information flow from the CC to the cerebellum is massively relayed via the pontine nuclei (Brodal, 1978; Glickstein et al., 1985; Leergaard, 2003; Legg et al., 1989). The ponto-cerebellar connection provides mossy fibers to the granule cells in the cerebellar cortex and collaterals to neurons in the CN (Biswas et al., 2019; Henschke & Pakan, 2020; Ruigrok, 2011), which is crucial in planning and coordinating fine precision movements of the forelimbs (Guo et al., 2020; Wagner et al., 2019).

In addition to the mossy fiber route, CC may also control cerebellar processing via their climbing fiber input, which is derived from the inferior olive (IO) (Burman et al., 2000; Kubo et al., 2018; Ramnani, 2006; Saint-Cyr, 1983). Whereas decades of neuroanatomical research have elucidated the intricate topographical relationship of the cortico-ponto-cerebellar connections (Brodal, 1978; Glickstein et al., 1985; Henschke & Pakan, 2020; Leergaard, 2003; Legg et al., 1989), much less is known about that of the cortico-olivocerebellar system. Direct cerebro-olivary connections are sparse (Berkley & Worden, 1978; Saint-Cyr, 1983) and the indirect connections are diverse, presumably including various secondary intermediaries in both the lower and higher brain stem (Berkley et al., 1986; Bull et al., 1990). Of particular interest in this respect is the mesodiencephalic junction (MDJ), as this area provides a particularly dense projection to the IO (De Zeeuw et al., 1989; Kubo et al., 2018; Leichnetz et al., 1984; Linauts & Martin, 1978; Mabuchi & Kusama, 1970; Nakamura et al., 1983a; Onodera, 1984; Rutherford et al., 1984; Swenson & Castro, 1983). This area around the fasciculus retroflexus (FR) includes, among others, the medial accessory nucleus of Bechterew and the nucleus of Darkschewitsch, and it targets particularly the principal olive and the rostral medial accessory olive (Figure S1) (De Zeeuw et al., 1989; De Zeeuw & Ruigrok, 1994; Onodera, 1984; Saint-Cyr, 1987; Voogd & Ruigrok, 2004). Next to an input from the CC, the MDJ also receives input from the CN (Bentivoglio & Kuypers, 1982; De Zeeuw & Ruigrok, 1994; Gonzalo-Ruiz et al., 1990; Rutherford et al., 1989; Saint-Cyr, 1987; Teune et al., 2000), raising the possibility that CC and CN conjunctively control olivary activity via this central hub in the brain stem. Despite all the evidence for its central strategic position in cerebro-cerebellar communication, several critical questions on the input-output relations of the MDJ remain to be elucidated. It is still unclear which olivary subnuclei receive inputs from which parts of the CC via which parts of the MDJ. In addition, it is also unclear whether the MDJ neurons that do receive input from the CC and project to the IO also receive a direct input from the CN, and if they do, from which parts of the CN. Moreover, in addition to these specific questions on the topography of the connections of MDJ neurons, it is also unclear how dense they are.

Here, we addressed these questions in mice by exploiting classical and advanced, retrograde and anterograde tracing approaches as well as by analyzing mesoscale cases of cortical anterograde injections from the Allen Mouse Brain Connectivity data set. We provide

Significance

The MDJ forms a central hub for cerebro-cerebellar communication via the olivary climbing fiber system. For the first time, using transneuronal rabies tracing, we provide direct evidence that olivary-projecting neurons in the MDJ receive inputs from both the cerebral cortex and the cerebellar nuclei. The inputs and outputs of the MDJ compartments turn out to be topographically organized relaying a precise organization of the cerebral cortical regions onto the different olivary subnuclei. Our findings provide fundamental, anatomical evidence for how the cerebrum instructs the cerebellum during sensorimotor and cognitive tasks.

CC-MDJ-IO as well as CN-MDJ-IO topographical and density input-output maps, and we show that CC and CN can converge their projections onto the same olivary-projecting MDJ neuron. These data establish the MDJ as an important central hub in widespread cerebro-cerebellar communication, supporting the integration of multiple loops engaging the IO.

2 | METHODS AND MATERIALS

2.1 | Animals and viral vectors

Both male and female C57BL/6J mice were used in this study (the mice used for the Allen Brain data set were already processed). Animals were 10–20 weeks old and were housed individually in a 12-hr light-dark cycle with food and water ad libitum. All experiments were approved by the institutional animal welfare committee of Erasmus MC (15-273-146 and 15-273-147) in accordance with Central Authority for Scientific Procedures on Animals Guidelines.

Adeno-associated virus AAV8-CAG-FLEX-TCB (Addgene plasmid #48332), AAV8-CAG-FLEX-oG (Addgene plasmid #74292), and rabies virus RV-CMV-EnvA-ΔG-eGFP (Addgene plasmid #32635) were obtained from Salk vector core. AAV1-CAG-GFP_{sm}-myc (Addgene plasmid #98926), AAV1-CB7-RFP (Addgene plasmid #105546), AAVretro-CAG-GFP (Addgene plasmid #105542), and AAVretro-hSyn-Cre-eBFP (Addgene plasmid #51507) were obtained from Addgene.

2.2 | Surgical procedures

Animals were anesthetized with 5% isoflurane for induction and 2.5% for maintenance and were fixed on a stereotaxic surgical plate (David Kopf Instruments). Body temperature was kept at $37 \pm 0.5^\circ\text{C}$ constantly during operation. DuraTears (Alcon Laboratories, Inc.) was used to moisture the eyes, and lidocaine (2.5 mg/ml) was locally

applied on the skin after removing hair over the scalp. A small vertical incision was applied on the scalp to expose the skull. Animal head was positioned so that the bregma and lambda were well leveled. Stereotaxic coordinates (Table S1) were measured for different injecting targets, then a small craniotomy ($\Phi = 0.7$ mm) was made on the skull. We gently lowered a glass capillary ($\Phi = 8$ μ m opening) in the targeted regions and slowly injected about 30 nl cholera toxin B subunit (CTB, 1%, Sigma-Aldrich, C9903) or virus. Capillaries were left on the injection sites for approximately 2 min before being removed from the brain. All the intracranial injections were performed unilaterally.

For CTB experiments (Figures 1, 3-5), animals were sacrificed 2 days postsurgically. For monosynaptic rabies experiment (Figure 6), helper virus (AAV8-CAG-FLEX-TCB and AAV8-CAG-FLEX-oG) and AAVretro-hSyn-Cre-eBFP were delivered simultaneously 4 weeks

prior to the rabies injection, and mice were sacrificed after 8 days following rabies injection. For the triple-tracing experiment (Figure 7), mice were allowed to survive for 3 weeks after viral injections.

2.3 | Immunohistochemistry

We deeply anesthetized animals by intraperitoneal injecting pentobarbital sodium solution (50 mg/kg) and perfused transcardially with saline, followed by 4% paraformaldehyde (PFA)-0.1 M phosphate buffer (PB, pH 7.4). Brains were freshly removed and post-fixed in 4% PFA-0.1 M PB for 2 hr at room temperature. Fixed brains were placed in 10% sucrose overnight at 4°C and were embedded in 12% gelatin-10% sucrose. After fixation in 10%

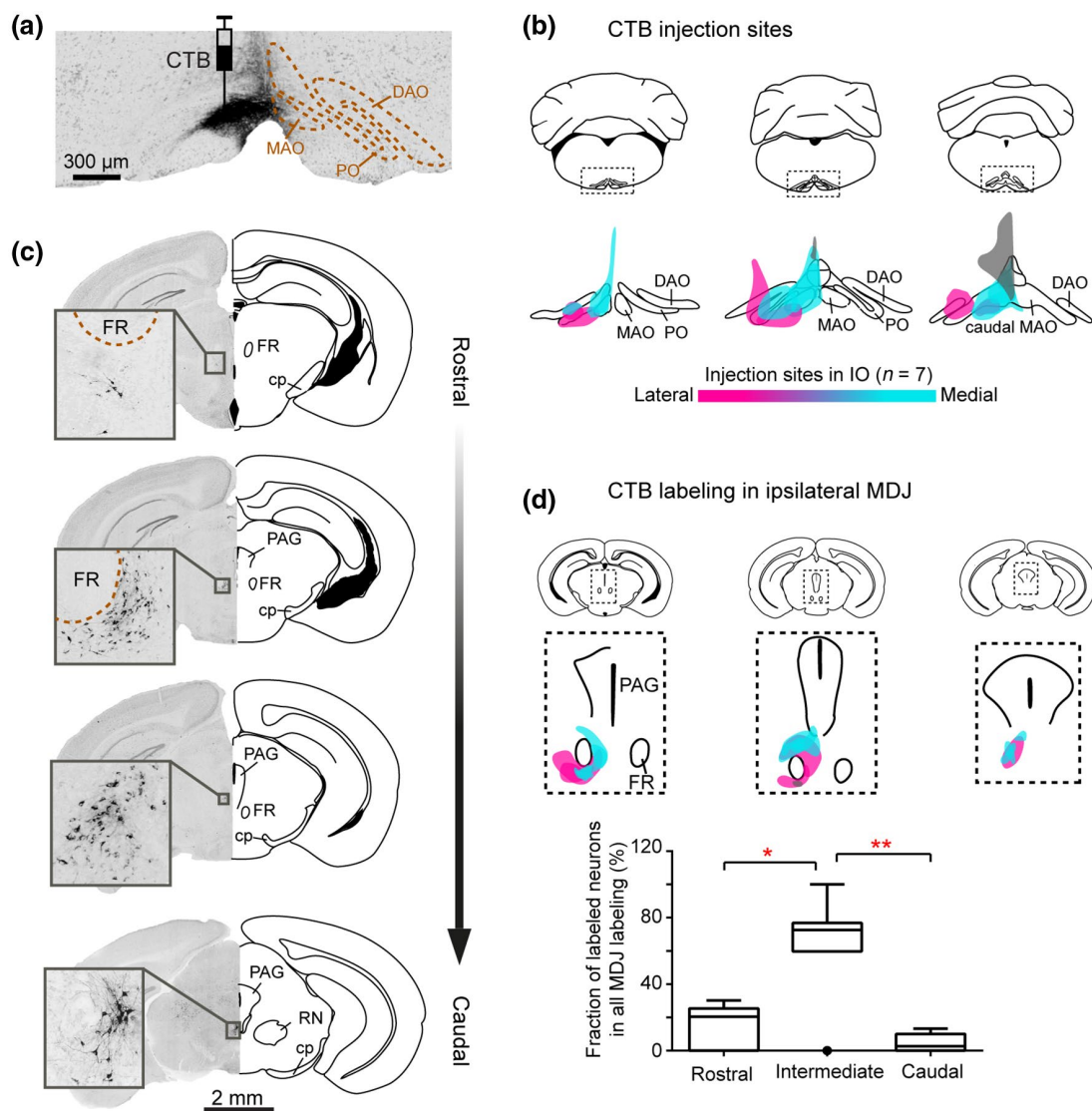


FIGURE 1 CTB injections in the IO retrogradely label MDJ neurons. (a) Coronal section of IO from a representative mouse, showing CTB injection in the MAO. (b) Summary of the IO injections for seven mice. Magenta, cyan, and gray: injections mainly cover PO ($n = 2$, magenta), rostral MAO ($n = 3$, cyan), and caudal MAO ($n = 2$, gray). (c) Retrogradely labeled neurons in the MDJ at four anteroposterior levels. Sections are obtained from the injection in (a). (d) Summary of CTB-labeled neurons in the MDJ regions (upper, overlay of seven mice) and their anteroposterior distribution (lower). Error bars denote standard deviation. * $p < 0.05$; ** $p < 0.01$

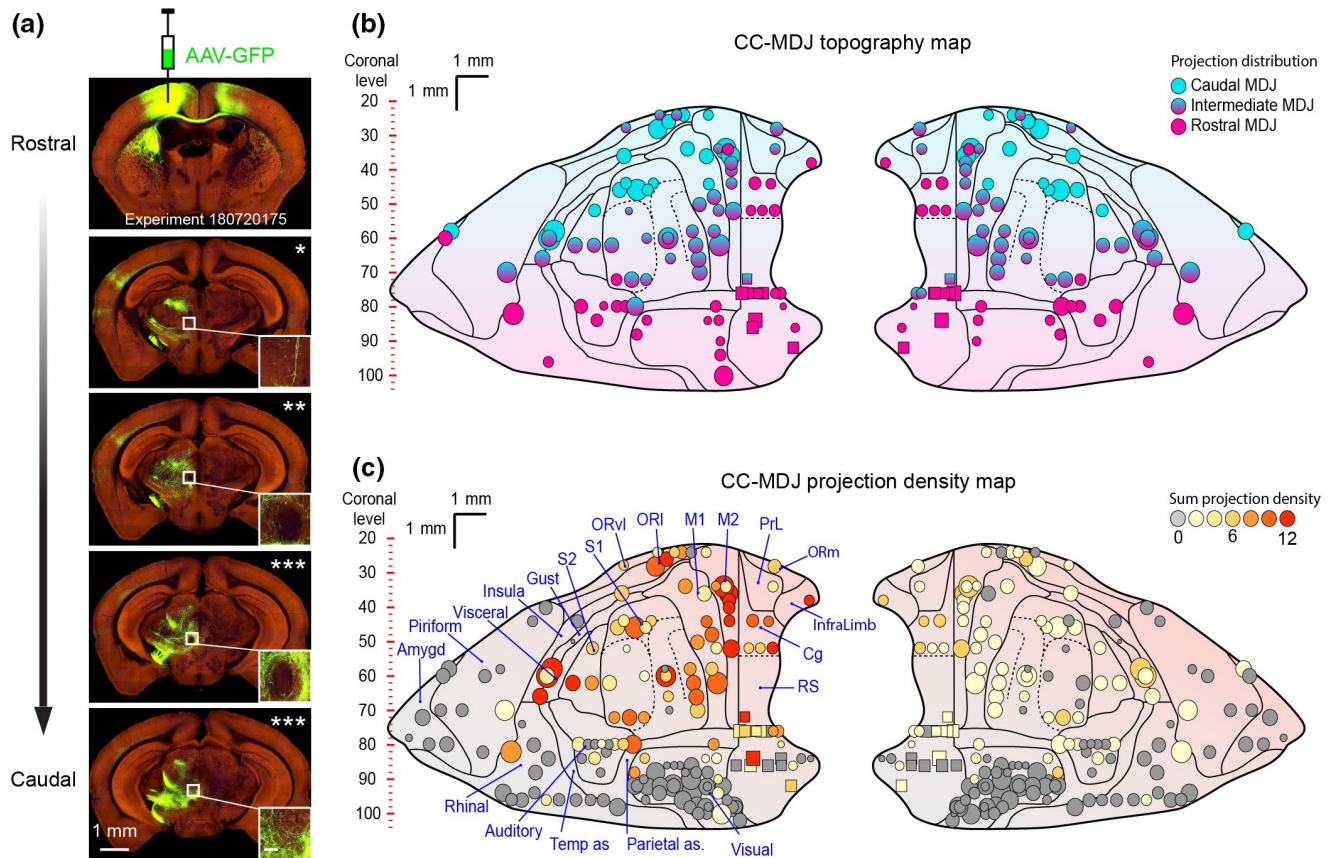


FIGURE 2 Viral anterograde tracing demonstrates CC-MDJ topographic and density organizations. (a) Images of an example case from the Allen Mouse Brain Atlas with an injection in the motor cortex (top) and projections at anteroposterior levels of the MDJ. The number of asterisks represents cortical axon density in the MDJ (inset, scale bar = 100 μ m, see quantification in the Materials and Methods). (b) CC-MDJ topography map of cortical injections on our standard flattened CC representation (Aoki et al., 2019). Each marker represents one injection in the CC (wild types in circle, $n = 83/167$; transgenics in squares, $n = 6/167$); marker size indicates injection volume (see Materials and Method); color coding suggests axonal projection in the anteroposterior MDJ. (c) CC-MDJ density map of cortical areas projecting onto the MDJ. The different density levels are represented by the color of the circles and squares on the standard flattened scheme of the CC. Note that the cases exhibiting no MDJ projection (gray markers, $n = 78/167$) were not illustrated in panel (b). Amygd, amygdala; Auditory, auditory cortex; Cg, cingulate cortex; Gust, gustatory cortex; InfraLimb, infralimbic cortex; Insula, insular cortex; M1, primary motor cortex; M2, secondary motor cortex; ORI, lateral orbital cortex; ORm, medial orbital cortex; ORvl, ventrolateral orbital cortex; Parietal as, parietal association cortex; Piriform, piriform cortex; PrL, prelimbic cortex; Rhinal, rhinal cortex; RS, retrosplenial cortex; S1, primary somatosensory cortex; S2, secondary somatosensory cortex; Temp as, temporal association cortex; Visceral, visceral cortex; Visual, visual cortex

formalin-30% sucrose overnight at 4°C, serial coronal sections were sliced with microtome (SM2000R, Leica) at 50 μ m and collected in 0.1 M PB.

For CTB immunohistochemistry, slices were incubated in goat anti-CTB subunit primary antibody (1:15,000, List labs, 703) overnight at 4°C and biotinylated horse anti-goat secondary antibody (1:2,000, Vector, BA-9500) for 2 hr at room temperature. Slices were incubated with ABC complex (volume ratio 1:1, Vector, AK-5200) for 1.5 hr at room temperature. Next, labeling was visualized with DAB staining (1:150), and slices were mounted for light microscopy. For GFP_{sm}-myc signal visualization, slices were incubated in goat anti-myc primary antibody (1:10,000, Abcam, ab9132) overnight at 4°C, followed by Cy⁵ donkey anti-goat secondary antibody (1:400, Jackson, 705-175-147) at room temperature. All slices for fluorescent microscopy were counterstained

with DAPI. All antibodies were diluted in 2% normal horse serum-0.4% Triton-0.1M PBS solution.

2.4 | Analyses of the injections from Allen Mouse Brain data set

For the retrieval analyses of cortical injections from the Allen Mouse Brain data set (<https://mouse.brain-map.org/>), we included 167 cortical injections ($n = 153$ wild type; $n = 14$ transgenic) that were accessible before June 2018. The viral vectors AAV-GFP and AAV-FLEX(DIO)-GFP were used for wild-type and transgenic mice, respectively. To map the precise cortical-MDJ topography, we selected the injections which were targeted the reported locations with least contamination in other regions. For each cortical

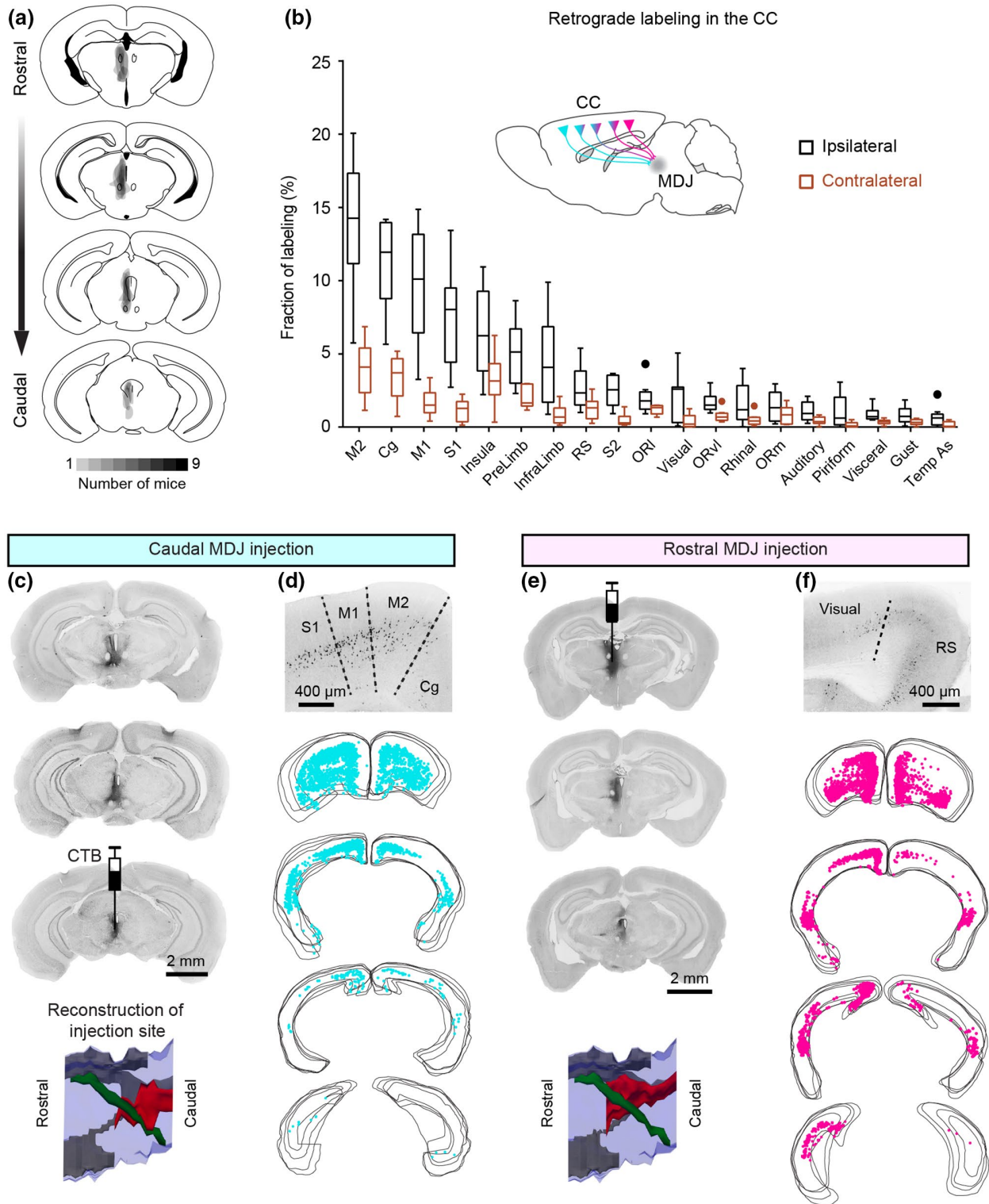


FIGURE 3 CTB retrograde tracing from the MDJ to the CC. (a) Summary of CTB injections in the MDJ regions ($n = 9$ mice). (b) Quantification of retrogradely labeled cells in the CC. Light gray and dark gray represent fractions of total labeled cells on the contralateral and ipsilateral sides, respectively. (c–f) Comparison of retrograde cortical labeling from a caudal MDJ-injected case and a rostral MDJ-injected case. In the lateral view of injection site reconstruction (bottom, c and e), red: CTB injection site, green: FR, gray: third ventricle, blue: midbrain contour. Example cortical sections (d and f) show CTB labeling ipsilateral to the injection sites. In the serial plotting of cortical labeling (d and f), each panel include four consecutive sections. See abbreviations in Figure 2

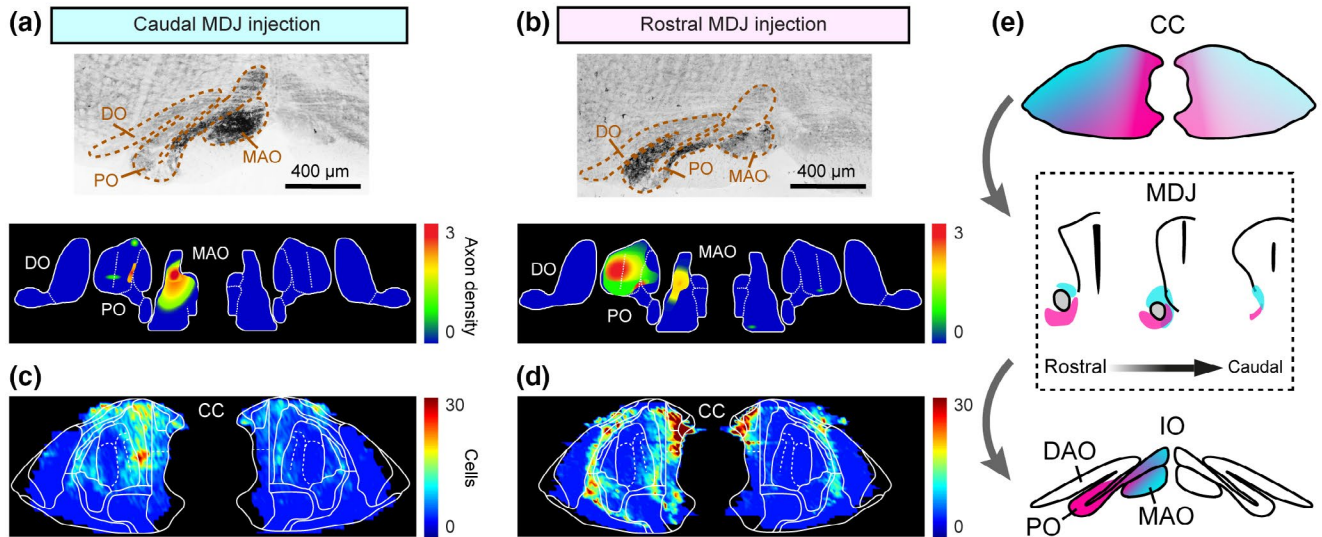


FIGURE 4 CC-MDJ-IO topography by injecting CTB in anteroposterior MDJ. (a and b) Example sections (upper) and density maps (lower) of anterogradely labeled MDJ axons in the IO. (c and d) Density maps of retrogradely labeled neurons in the CC from the caudal and rostral MDJ injections. (e) Schematic of CC-MDJ-IO topographic organization. DO, dorsal accessory olive; MAO, medial accessory olive; PO, principal olive

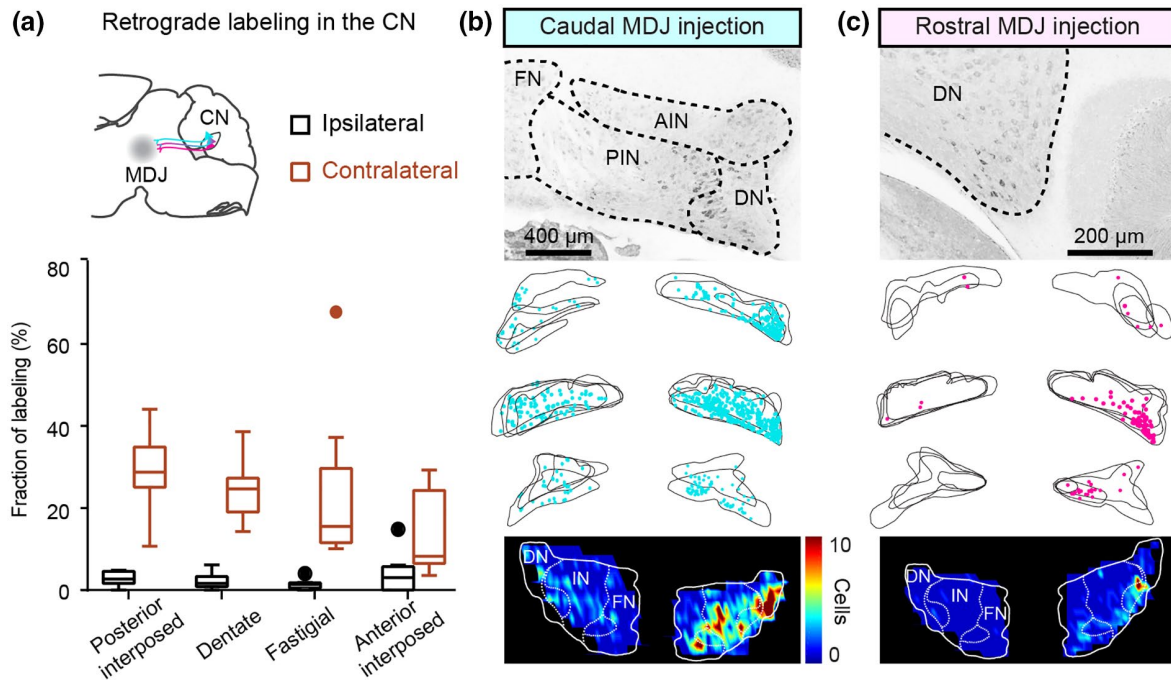


FIGURE 5 Retrograde CTB labeling from the MDJ to the CN. (a) Summary of CTB-labeled neurons in the CN ($n = 9$ mice). (b and c) Comparison of retrograde CN labeling from a caudal MDJ-injected case and a rostral MDJ-injected case. Example sections show labeling in the contralateral CN. In the serial plotting of CN labeling, each panel is overlaid with two to four consecutive sections. Note the variability of positional matching in the serial plotting is due to imperfect coronal sectioning. Labeling density is illustrated in the color maps (lower) for both cases

area, we included at least one wild-type mouse except for the retrosplenial cortex; for this region that there were no appropriate injections in wild types available at the time, and hence to analyze this area we included 14 transgenic mice. For detailed information of each injection, please see the repository <https://github.com/XiaoluOne/MDJ>.

Based on the given volume, we transformed the injections into circles for wild-type mice or squares for transgenic mice with the radius formula: $r = 10 \times \sqrt[3]{3 \times \text{injection volume} / 4\pi}$. Next, we plotted each injection on a standard flattened cortical map in line with the stereotaxic coordinates of the injections. To map the MDJ projection density on the cortical map (Figure 2c), we assessed

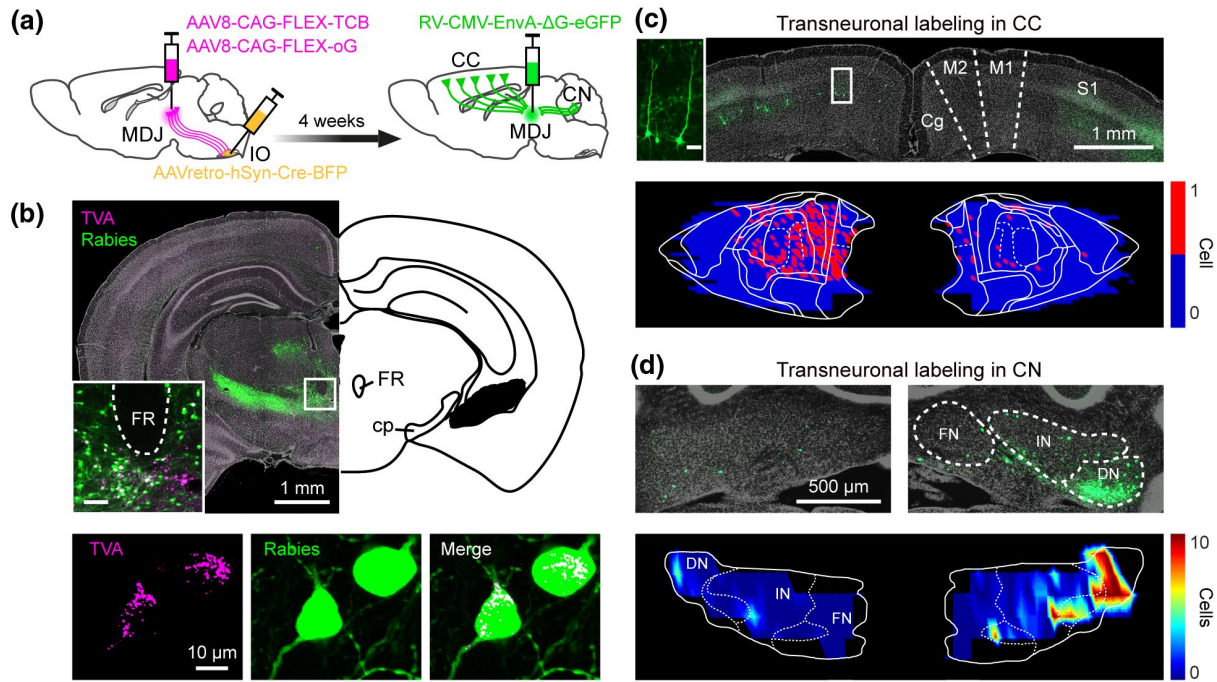


FIGURE 6 Monosynaptic rabies tracing revealing CC and CN inputs on the olivary-projecting MDJ neurons. (a) Schematic of transneuronal viral-tracing strategy ($n = 4$ mice). (b) Coronal sections of a representative mouse at the midbrain level (upper, inset suggesting MDJ, inset scale bar = 100 μm), showing rabies primary labeling (lower, TVA and rabies co-labeled) and local secondary labeling. (c) Coronal section (upper) and plotting map (lower) of transneuronal rabies labeling in layer-5 pyramidal cells (inset, scale bar = 50 μm) of motor cortex. (d) Same as (c), but for labeling in the CN. DN, dentate nucleus; FN, fastigial nucleus; IN, interposed nucleus

the cortical axon density on four coronal sections (two-photon tomography at $5,000 \times 3,750$ resolution) along the anteroposterior axis of the MDJ by scoring 0–3 for each section, yielding a value ranging from 0 to 12 for each mouse (see e.g., in Figure 2a). All injections were color-coded based on the sum of density scores. To plot topographic organization of the MDJ projections on the cortical map (Figure 2b), we colored each case based on the relative anteroposterior location of the MDJ sections that exhibiting most abundant cortical projection (magenta for rostral, mix for intermediate, and cyan for caudal MDJ projection). The cortical injections that provided no labeled axons in the MDJ were represented in gray in the density plots (Figure 2c) but removed in the topography plots (Figure 2b) to optimize visualization.

2.5 | Microscopy and analyses

All overview sections were imaged with either a bright-field microscope (Nanozoomer 2.0-RS, Hamamatsu) or a fluorescent microscope (Axio Imager 2, ZEISS), and higher magnification images were captured with a confocal microscope (LSM 700, ZEISS) for further quantification. For plotting the brain contours and labeling, we either imported brain images (from fluorescent sections) or used an Olympus microscope equipped with a Lucivid miniature monitor and manually plotted with NeuroLucida software (MicroBrightfield, VT, USA). We used serial sections with 100 μm intervals to plot as

well as quantify labeling in the CN, the IO, and the MDJ areas. Serial sections with 200 μm intervals were used for quantification and plotting of cortical neurons. To quantify the CTB-labeled neurons in the MDJ, we firstly identified the subnuclei of the MDJ (Figure S1), then manually counted the labeled neurons with ImageJ.

Standard flattened maps of the CC, the CN, and the IO were made by transforming the mouse brain atlas (Paxinos & Franklin, 2019), which was described in detail in our previous work (Aoki et al., 2019; Ruigrok & Voogd, 2000; Suzuki et al., 2012). To present CTB- and rabies-labeled cells on color-coded flattened maps of the CC and the CN, we first reconstructed the contours of these structures and plotted the labeled cells, then superimposed sections with 200- μm bins for the CC and 100- μm bins for the CN. Retrogradely labeled cells were counted in each bin, resulting in numeric matrices for the MDJ projection cells in the CC and CN. For the IO colormap, we first marked the border of MDJ axon on each olivary section; next, we subjectively scored the axon density as 0–3 and illustrated on the standard flatten map of the IO. All colormaps were plotted using MATLAB 2017a (RRID:SCR_001622).

To quantify the fraction of olivary-projecting MDJ cells (GFP) overlapping with CC and CN axons (Figure 7c), we applied thresholding (85th–95th percentiles) to binarize these images and then overlaid GFP channel with the other two channels to calculate the colocalization and overlapping area fraction. To examine the CC/CN terminations on the olivary-projecting MDJ neurons (Figure 7d), we acquired z-stack confocal images (0.35 μm sectioning) for the MDJ

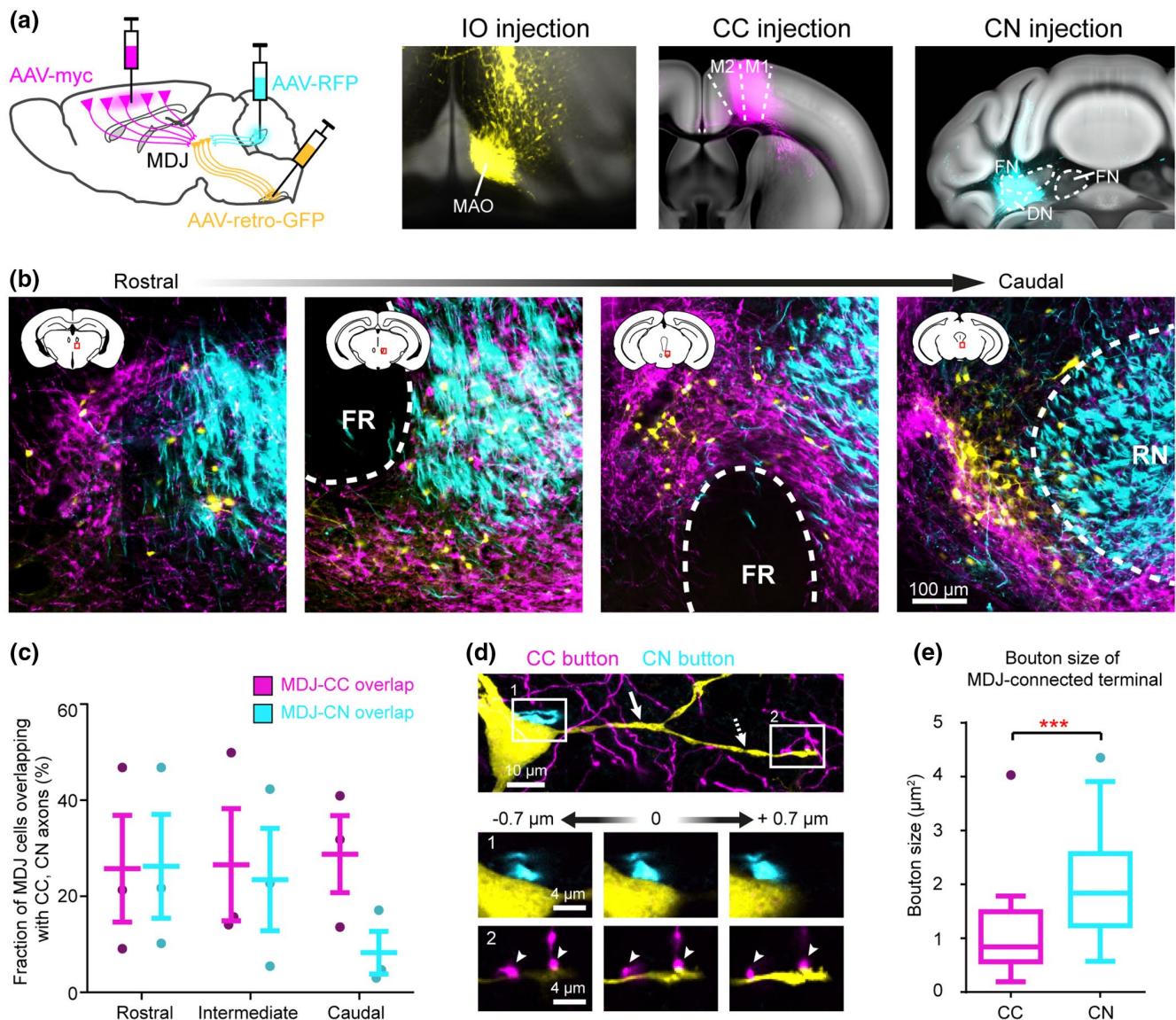


FIGURE 7 Convergence of CC and CN terminations on the olivary-projecting MDJ neurons. (a) Schematic of tracing strategy. Coronal sections (registered in the Allen CCF) showing injections of retrograde AAV-GFP in the IO, anterograde AAV-myc in the motor cortex, and AAV-RFP in the cerebellar interposed-dentate complex. (b) Coronal sections of MDJ regions from an example mouse showing retrogradely labeled cells (olivary-projecting cells, yellow) distributing in the CC (magenta) and CN (cyan) axons. (c) Colocalization quantification of olivary-projecting cells and CC, CN axons at anteroposterior MDJ levels ($n = 3$ mice, plotted as mean \pm SD). (d) Confocal images of an olivary-projecting MDJ neuron from (b) showing close synaptic contact with CN axon on its soma (inset 1) and with CC axons on its secondary dendrite (inset 2). Solid arrow: primary dendrite, dashed-line arrow: secondary dendrite. (e) Size comparison of CC and CN boutons exhibiting close contacts with IO-projection MDJ cells ($n = 27$ for CC boutons, $n = 37$ for CN boutons, $t_{(62)} = 3.67$, $***p < 0.001$)

regions. Synaptic contacts were defined as colocalizations from orthogonal views at more than three different z planes. To quantify the CC/CN bouton sizes (Figure 7e), we first binarized and applied threshold (85th–95th percentiles) to the maximum intensity projection images of these boutons; next, bouton areas (μm^2) were calculated by summing the bright pixels and transformed based on the image magnification. All image quantification was performed by using ImageJ. Statistical analyses were performed by using GraphPad Prism 6.0 (RRID:SCR_002798), and statistical significance was defined as $p < 0.05$. All graphs are plotted using Tukey method box and whiskers unless specified otherwise.

3 | RESULTS

3.1 | Projection from MDJ to IO

In mammals, the MDJ is recognized as a dome-shaped area wrapping around the FR at the border of the mesencephalon and diencephalon (Carlton et al., 1982; Onodera, 1984). In the current study on the murine MDJ, we adhere to the terminology in higher mammals such as cats (Burman et al., 2000; Onodera, 1984; Onodera & Hicks, 2009; Strominger et al., 1979), for which the subregions of the MDJ have been more accurately and consistently described

than in rats (Brown et al., 1977; Ruigrok et al., 2004; Rutherford et al., 1984). More specifically, the MDJ in mice forms a continuous rostrocaudal cell column, starting rostrally at the prerubral field (PR) and rostral interstitial nucleus of the medial longitudinal fasciculus (RI) located ventrally to the FR, dwindling medially covering areas of the medial accessory nucleus of Bechterew (NB) and the nucleus of Darkschewitsch (Dk), and ultimately transcending dorsally and caudally on the border of the periaqueductal gray (PAG) in the interstitial nucleus of Cajal (InC) and medial accessory oculomotor nucleus (MA3) (Figure S1). Instead, the murine IO is located in the ventral medulla oblongata and consists, just like those of all other mammalian species, of several sheaths of neuropil that form separate subnuclei, including the principal olive (PO), medial accessory olive (MAO), and dorsal accessory olive (DAO) (De Zeeuw et al., 1998).

To uncover the precise topography of the MDJ projection to the IO in mice, we started with retrograde tracing experiments by injecting 1% CTB solution unilaterally in the different olivary subnuclei ($n = 7$ mice, Figure 1a,b). In addition to some scattered labeling throughout the midbrain, we observed compact, yet overlapping, retrogradely labeled cell populations distributed across various subregions of the ipsilateral MDJ, extending for approximately 1.2 mm in the sagittal plane (Figures 1c,d and S2). In most cases, retrogradely labeled neurons were situated along the rostrocaudal cell column of the PR, RI, NB, Dk, InC, and MA3 (Figure 1c,d and Video S1). The injections that covered the PO received the most prominent projections from the rostroventral subregions of the MDJ, whereas those in the rostral MAO resulted in more retrograde labeling in the more intermediate and caudal subregions of the MDJ (Figure S2). These findings were corroborated by analyses of the outcomes of the injections that were made with the use of different stereotactic coordinates in the rostrocaudal plane.

Notably, no or only very few retrogradely labeled cells were observed within the confines of the magnocellular red nucleus (Figure 1c,d), which is in line with an earlier description in rat (Ruigrok et al., 2004; Rutherford et al., 1984). In addition to the topographical differences highlighted above, we observed slight differences in the densities of the projections. When we quantified the CTB-labeled cells at distinct rostrocaudal levels of the MDJ in the seven mice, we observed that labeling was most abundant at the intermediate level, comprising the medial accessory nucleus of Bechterew and nucleus of Darkschewitsch (Figure 1d, intermediate vs. rostral and caudal level, one-way ANOVA, Tukey's multiple comparisons test, $F(1.2, 7.1) = 21.02, p = 0.002$).

Given that some of our injections diffused slightly into some of the adjacent structures of IO, that is, the reticular formation of the medulla oblongata, we did additional control experiments in which we injected CTB in the overlying caudal gigantocellular and paramedian reticular nucleus, while avoiding the IO ($n = 2$ mice, Figure S3a). In these experiments, we observed only few CTB-labeled cells in the caudal MDJ (Figure S3b), indicating that the MDJ projections described above presumably indeed target virtually exclusively the IO. All together, we conclude that in the mouse a topographic projection from the MDJ to PO and rostral MAO can be recognized, similar to that in the cat (Onodera, 1984).

3.2 | Projection from CC to MDJ

As the projections from the MDJ subregions to the IO subnuclei are organized in a topographical manner (Figure 1), we wanted to find out to what extent the projection from the CC to the MDJ is similarly organized. To this end, we first exploited data gathered for the generation of the Allen Mouse Brain Connectivity Atlas (Allen Atlas in short). This data set consists of anterograde AAV-GFP viral tracing from various areas of the CC to downstream structures in both wild-type (circles) and transgenic mice (squares) (Oh et al., 2014). In our analyses ($n = 167$ mice), we focused on the cases in which a projection from the CC to the MDJ could be observed ($n = 89/167$ mice), taking the injection volumes into account (see Materials and Methods for details). We first plotted the CC injections dependent on the rostrocaudal projection of terminals that they provided in the MDJ (Figure 2a), yielding the overall topography on a flattened map of the mouse CC (Figure 2b) (Aoki et al., 2019). Along the 1.2-mm longitudinal axis of the MDJ, the caudal MDJ, comprising InC and MA3, receives most of its projections from relatively rostralaterally located parts of the ipsilateral CC (e.g., rostral parts of the primary and secondary motor cortices as well as primary and secondary somatosensory cortices; see cyan markers in Figure 2b); whereas axon terminals in the rostral MDJ, covering parts of the PR and RI, originate mainly from injections in either the medial and caudal parts of the ipsilateral CC (e.g., cingulate, retrosplenial, and infralimbic cortices as well as specific parts of the auditory and visual cortex; see magenta markers). The intermediate subregions of the MDJ, including NB and DK, also receive input from parts of the primary and secondary motor cortices as well as primary and secondary somatosensory cortices, but those are situated posterior to the analogous sources of the CC that project to the caudal MDJ (see structures in Figure 2b marked with mixed cyan and magenta colors). In addition to all these prominent ipsilateral projections, there were also many contralateral projections. Interestingly, the topography of these contralateral projections was virtually all symmetric to the ipsilateral ones, highlighting the relevance of bilateral control (Figure 2b, right panel).

To estimate the relative prominence of the MDJ projections from the different cortical regions, we presented the density of these projections of the Allen Atlas with color coding onto the same map. The most densely labeled terminal fields covering the MDJ resulted from mice with injections in the ipsilateral infralimbic, cingulate, secondary motor, sensory, lateral orbital, gustatory, and/or visceral cortical areas, but the injections in many of the other areas also resulted in some labeling of efferent axons located in the ipsilateral MDJ ($n = 89$ mice, colored markers in Figure 2c). In contrast, many injections in various parts of the CC resulted in no labeling of the MDJ; these included, for example, specific parts of the piriform, visual, auditory, and parts of the somatosensory cortices ($n = 78$ mice, gray markers in Figure 2c). Finally, the contralateral CC-MDJ projections showed a consistently lower number of efferent fibers than the ipsilateral ones (Figure 2c). Hence, by evaluating a large number of cases, our retrieval analyses yielded the CC-MDJ projection maps, establishing their topographic relations and density "hot spots."

Next, we wanted to verify the anterograde approach of the Allen Atlas with retrograde tracing experiments. To this end, we performed small unilateral CTB injections ($n = 9$) targeting the MDJ region at the various caudorostral levels (Figures 3a and S4) and examined the retrograde labeling in the CC (Figure 3b). In addition to some retrogradely labeled cells in the lateral habenular nucleus, pre-commissural nucleus, parafascicular thalamic nucleus, and posterior paraventricular thalamic nucleus, CTB-labeled cells were observed in various CC regions predominantly, but not exclusively, on the ipsilateral side (Figure 3b). Virtually all labeled cells in the CC were found in the layer 5 (Figure 3d,f). In terms of distribution density, cortical labeling was in general most abundant in the motor, cingulate, primary somatosensory, insula, prelimbic, and infralimbic cortices, labeling more than 5% of the total CTB-labeled neurons in the CC (Figure 3b). The injections at the caudal and rostral level of the MDJ showed relatively high numbers of retrogradely labeled cells in the rostrolateral and medial areas of the CC, respectively (compare Figure 3c,d with Figure 3e,f, respectively). For example, the CTB injections in the caudal and rostral MDJ provided particularly robust retrograde labeling in parts of the motor and cingulate cortices. These results are in line with the topography and density maps of the CC-MDJ projection revealed with anterograde tracing (Figure 2).

Given that some of the CTB injections also included the parafascicular thalamic nucleus and PAG, which are known to receive afferent projections from the cingulate, prelimbic, and infralimbic cortices (An et al., 1998; Cornwall & Phillipson, 1988; Gonzalo-Ruiz et al., 1990; Mandelbaum et al., 2019; Royce et al., 1991; Teune et al., 2000), we did additional control experiments by targeting these nuclei selectively without hitting the MDJ (Figure S5a). In principle, these nuclei might also constitute an intermediary hub between the CC and the IO. In these control injections surrounding the MDJ, we did indeed observe abundant retrograde labeling in the cingulate and limbic cortices as well as in the medial prefrontal cortex, but we hardly observed any axonal labeling in the IO (Figure S5b,c), excluding the possibility that the parafascicular thalamic nucleus and adjacent PAG form major hubs between the CC and IO. Taken together with the anterograde experiments from the CC described above (Figure 2), our retrograde tracing experiments highlight that the projection from the CC to the MDJ concerns very large, but not all, parts of the CC and that this input is topographically organized and dense. Additionally, it is essential to use both anterograde and retrograde tracing methods to elucidate the connectivity of the CC with the IO via the MDJ and to avoid potential caveats.

3.3 | Topographic connectivity between CC, MDJ, and IO

To be able to better compare the topography of the inputs from the CC to the different MDJ regions with that of the MDJ outputs to the IO, we next plotted the anterograde labeling in the different olivary subdivisions (Figures 4 and S4), exploiting the fact that CTB can be used not only as a retrograde but also an anterograde tracer

(Angelucci et al., 1996; Conte et al., 2009). The CTB injections at the rostral and caudal levels of the MDJ showed relatively high numbers of anterogradely labeled fibers in the ipsilateral PO and rostral MAO, respectively (compare e.g., Figure 4a,b). Interestingly, the fibers that traversed from the rostral MDJ to the PO appeared to be routed via the central tegmental tract, whereas those of the caudal MDJ traveling toward the rostral MAO were predominantly located in the medial tegmental tract, which is in line with earlier descriptions in monkeys and cats (Burman et al., 2000; Ruigrok et al., 2004). When putting the data provided by the injections in the IO (Figure 1), the CC (Figure 2), and MDJ (Figures 3 and 4), together, the picture emerges that the rostromedial and caudal parts of the CC predominantly project to the PO via the PR and RI, that the rostrolateral parts of the CC predominantly project to the rostral MAO via the InC and MA3, and that the in-between parts of the CC predominantly project to overlapping parts of the PO and MAO via the BN and DK (Figure 4e).

3.4 | Projection to MDJ from CN

The CTB injections in the MDJ described above also provided substantial retrograde labeling in the contralateral CN (Figures 5a–c and S4). More specifically, the rostral and caudal MDJ injections resulted in retrogradely labeled cells in predominantly the contralateral dentate nucleus (DN) and posterior interposed nucleus (PIN), respectively (Figure 5b,c). Each of them resulted in more than 25% of the total CN labeling (Figure 5a). Approximately 15% of the total CN labeling was found in the anterior interposed nucleus (AIN), including the dorsolateral hump (Figure 5a). Notably, the variability of retrograde labeling was relatively high in the fastigial nucleus (FN) (SD in FN = 18.7 vs. 9.2, 9.8, and 7.1 in the PIN, AIN, and DN, respectively). This may partly reflect the fact that two of the nine injections in the MDJ regions diffused into the oculomotor area and PAG, which are known to receive abundant FN input (Fujita et al., 2020; Gonzalo-Ruiz et al., 1990; Teune et al., 2000). When we excluded these two animals which the injections largely spread in the oculomotor as well as the PAG areas, the other seven mice showed less labeling in the FN ($15.1\% \pm 4.9\%$ of the total cerebellar labeling, mean \pm SD).

3.5 | CC and CN projections converge onto MDJ neurons projecting to IO

Our CTB injections in the MDJ simultaneously provided retrograde labeling of cells in the CC and CN as well as anterograde labeling of axonal fibers in the IO (Figures 3–5). This raises the possibility that IO-projecting neurons in the MDJ may function as a central hub in the brain stem, onto which both CC and CN converge. To further clarify the relationship between MDJ input and output, we used a gene-modified transneuronal rabies strategy (Callaway & Luo, 2015; Kim et al., 2016; Wall et al., 2010), in which we retrogradely traced neurons in the CC and CN that send axon terminals to the MDJ cells

projecting to the IO ($n = 4$ mice). We first injected Cre-dependent helper virus AAV8-CAG-FLEX-TCB and AAV8-CAG-FLEX-oG in the MDJ and AAVretro-hSyn-Cre-eBFP in the ipsilateral IO, allowing MDJ neurons that project to the IO to express both rabies glycoprotein (oG) and avian acceptors (TVA) (Figure 6a). Next, following 4 weeks of incubation, we injected glycoprotein gene-deleted rabies pseudotyped with the avian sarcoma leucosis virus glycoprotein EnvA (RV-CMV-EnvA- Δ G-eGFP) in the MDJ to induce cell-specific, retrograde transneuronal labeling (Figure 6a). Indeed, after another week of incubation, rabies transfected a group of MDJ neurons (starter cells) that expressed TVA on their membranes (Figure 6b). The location of these starter cells was in accordance with that of the IO-projecting MDJ neurons (Figure 1), that is, a cell column surrounding the FR (Figure 6b). Transsynaptic retrograde rabies labeling was found in a variety of regions located at different distances. At short distance, we observed labeling in the zona incerta, the prerubral field, and the posterior commissure nuclei (Figure 6b), while at longer distances, we found labeling in both the CC and CN (Figure 6c,d). The retrogradely labeled cells in the CC and CN were located predominantly on the ipsilateral and contralateral side to the MDJ, respectively. In the CC, these comprised only layer-5 pyramidal neurons with their characteristic angular-shaped somata, multipolar dendritic trees, and elongated axons (Figure 6c); these neurons were distributed in specific parts of multiple cortical regions, including, for example the sensory, motor, cingulate, and retrosplenial cortices (Figure 6c). In the CN, these comprised the larger, presumably excitatory, neurons in the DN and PIN (Figure 6d). Thus, in line with the analyses of the Allen Atlas data and the CTB experiments described above (Figures 2–5), the transneuronal rabies-tracing experiments demonstrated the existence of IO-projecting neurons in the MDJ that receive direct input from the CC and also the existence of IO-projecting neurons in the MDJ that receive direct input from the CN.

The experiments described above provided supportive evidence for the MDJ to operate as a CC-CN converging hub, but they did not allow us to unequivocally address whether individual IO-projecting neurons in the MDJ can receive input from both the CC and CN. To explore whether CC and CN axons can converge onto the same olivary-projecting MDJ neurons, we performed triple viral-tracing experiments ($n = 3$ mice) combining retrograde tracing of AAVretro-GFP from the IO with anterograde tracing of AAV1-CAG-GFP_{sm}-myc and AAV1-CB7-RFP in the CC (motor cortex) and CN (DN and PIN), respectively (Figure 7a). AAVretro-GFP virus was taken up by the MDJ axons in the IO and subsequently transported retrogradely to the somata of neurons in MDJ areas that also received input from anterogradely labeled axons derived from the CC and/or CN (Figure 7b). Even though the inputs from the CC and CN to the most caudal tip of the MDJ were partly segregated, in the more rostral and intermediate subregions of the MDJ there was a prominent convergence of CC and CN inputs to olivary-projecting neurons (see e.g., 2nd panel on the left of Figure 7b with prominent triple labeling in NB). This conclusion was supported by quantification of the fractions of IO-projecting MDJ cells that received input from CC or CN axons at the different rostrocaudal levels (Figure 7c). Moreover,

we found the same topographic distribution of terminals derived from the various CC areas and CN areas as found following AAV-GFP and CTB injections (Figures 2 and 5, respectively). It is hard to exclude that some of the light microscopic profiles in the MDJ were false-positively interpreted as axon terminals (instead of passing fibers), but we are rather confident that most of the CC versus CN identifications were correct because of their peculiar postsynaptic distribution and size. Indeed, whereas CC boutons were mostly apposed to secondary dendrites, CN axon terminals preferably terminated on the somata and primary dendrites of MDJ neurons (Figure 7d). Likewise, the average size of CC boutons terminating on IO-projecting neurons in the MDJ ($1.07 \pm 0.76 \mu\text{m}^2$, mean \pm SD, $n = 27$) was significantly smaller (two-sample t test, $t_{(62)} = 3.67$, $p < 0.001$) than that of CN boutons ($2.22 \pm 1.48 \mu\text{m}^2$, mean \pm SD, $n = 37$) (Figure 7e), which is in line with that of previous electron microscopic studies (De Zeeuw & Ruigrok, 1994). Taken together, our triple-tracing experiments indicate that axon terminals originating from the CC and the CN can converge onto the same individual IO-projecting neurons in the MDJ, yet with differential distribution patterns at the subcellular level.

4 | DISCUSSION

When considering how the CC may influence cerebellar activity, the first major hub that comes to mind is the pons, which is the main source of mossy fibers for the cerebellum (Coffman et al., 2011; Henschke & Pakan, 2020; Ruigrok et al., 2004). The pons receives prominent topographic projections from a wide variety of cortical regions (Leergaard, 2003; Leergaard et al., 2000; Wiesendanger & Wiesendanger, 1982) and has been shown to exert a powerful control over the lateral hemispheres of the cerebellar cortex and DN during various types of behaviors, including planning and coordination of limb and eye movements (Chabrol et al., 2019; Guo et al., 2020; Ohmae et al., 2017). Here, we show unique topographic projections from the CC to the cerebellar cortex via the MDJ and IO, providing the climbing fibers to the Purkinje cells in the cerebellum. Exploiting advancements in transneuronal viral-tracing approaches as well as emerging large-scale databases on brain connectivity (Allen Atlas), we have been able to elucidate the topography of both the CC-MDJ-IO loop and the CN-MDJ-IO loop. Our data obtained in mice expand on existing data on the individual connections between CC and MDJ, CN and MDJ, as well as between MDJ and IO in a wide variety of species. More specifically, we demonstrate that rostromedial and caudal parts of the CC project predominantly to ventrorostral parts of the MDJ, which in turn provide a dense projection to the PO, whereas the more rostrolateral parts of the CC project predominantly to the caudodorsal parts of the MDJ, which in turn target predominantly the rostral MAO. The topography of this CC-MDJ-IO loop aligns well with that of the CN-MDJ-IO loop (De Zeeuw & Ruigrok, 1994). Whereas the DN receiving climbing fiber collaterals from the PO projects most prominently to the rostral MDJ, the PIN, which receives its collaterals from the rostral MAO,

projects most prominently to the caudal MDJ. Together, these findings highlight that the integration of cerebral cortical with cerebellar information is not only mediated by a loop via the pontine mossy fiber system, but also by MDJ loops engaging the olivary climbing fiber system.

4.1 | Topography of CC-MDJ-IO loop

By systematically analyzing a large number of cases with cortical anterograde viral injections from the Allen Mouse Brain data set and verifying this by performing retrograde CTB in the MDJ, we identified the topography of the cortical regions that provide input to the MDJ. In general, the rostromedial and caudal parts of the CC predominantly project to the rostroventral areas of the MDJ and the more rostralateral parts of the CC prominently project to the caudodorsal areas of the MDJ. Our CTB injections in the rostral and caudal aspects of the MDJ in mice are in line with earlier results obtained in monkey (Leichnetz et al., 1984), cat (Nakamura et al., 1983b; Onodera & Hicks, 1996; Rutherford et al., 1989; Saint-Cyr, 1987), rat (Hoover & Vertes, 2007; Murphy & Deutch, 2018), as well as mice (Kubo et al., 2018; Oh et al., 2014), as the most prominently distribution of retrogradely labeled cells were found in the somatosensory, motor, and premotor cortices as well as the cingulate and prefrontal areas.

Likewise, the topographic connections we showed here between the MDJ and IO for mice have also been studied in different species such as monkey (Burman et al., 2000; Onodera & Hicks, 2009; Strominger et al., 1979), cat (Mabuchi & Kusama, 1970; Onodera, 1984; Saint-Cyr, 1987; Saint-Cyr & Courville, 1981), and rat (Carlton et al., 1982; Rutherford et al., 1984; Voogd & Ruigrok, 2004). In cat, retrograde tracing studies from selective areas of the IO complex have demonstrated subpopulations of labeled neurons in the MDJ area, distributed over a wide variety of nuclei, including the parvocellular red nucleus, medial accessory nucleus of Bechterew, nucleus of Darkschewitsch, supratubal reticular formation, nucleus of the fields of Forel, and interstitial nucleus of Cajal (Condé & Condé, 1982; Onodera, 1984; Onodera & Hicks, 2009; Saint-Cyr & Courville, 1981; Walberg & Nordby, 1981). For example, areas like the medial accessory nucleus of Bechterew and the nucleus of Darkschewitsch project prominently to the PO and rostral MAO, respectively (Onodera, 1984). Studies in human (Burman et al., 2000; Massion, 1967; Onodera & Hicks, 2009) and nonhuman primates (Burman et al., 2000; Onodera & Hicks, 2009; Strominger et al., 1979) reported results that are largely comparable to those in the cat. Interestingly, in primates the tract that carries the fibers from the parvocellular red nucleus projecting to the PO, the central tegmental tract, has expanded proportionally, standing out against the medial tegmental tract that holds the fibers traversing from the nucleus of Darkschewitsch to the rostral MAO (Burman et al., 2000; Voogd & Ruigrok, 2004). Here, in mice, we find a similar location of the fibers traversing from the rostral MDJ to the PO, next to those traversing from the caudal MDJ to the rostral MAO, but this route

does not show the evolutionary expansion of the central tegmental tract seen in higher mammals, such as cats, monkeys, and human. In our view, the prominent topography in the connectivity between CC, MDJ, and IO as well as the expansion of the parvocellular red nucleus and the central tegmental tract in higher mammals underscores the emerging relevance of the MDJ as an intermediary hub in cerebro-cerebellar processing.

4.2 | Topography of CN-MDJ-IO loop

Our tracing experiments showed that the olive-projecting cells in the MDJ receive not only topographically organized inputs from different areas of the CC, but also inputs from the CN in an analogous way. In general, our findings in mouse are consistent with previous tracing results in rat (Bentivoglio & Kuypers, 1982; Berretta et al., 1993; Ruigrok & Teune, 2014; Teune et al., 2000), cat (De Zeeuw & Ruigrok, 1994; Fukushima et al., 1986), and monkey (Gonzalo-Ruiz et al., 1988; Kalil, 1981; Stanton, 1980), showing that the cerebellar projections onto the MDJ nuclei are also topographically organized. The cells in the rostral MDJ that get input from rostromedial and caudal parts of the CC receive inputs from predominantly the DN, whereas the neurons in the caudal MDJ that are more prominently connected with rostralateral parts of the CC mainly receive input from the interposed nucleus. These findings on the topography were corroborated by the density studies following CTB injections in the MDJ, in which we found that the amount of retrogradely labeled cells in the CN was positively correlated with the amount of anterogradely labeled terminals in the IO. Moreover, the reciprocal connections between the different CN and olivary subnuclei are also in line with the topography described above in that the DN is mainly connected with the ventral and dorsal lamellae of the PO (Apps & Hawkes, 2009), which receives input from the rostral MDJ, and that the interposed nucleus is mainly connected with the rostral MAO (Apps & Hawkes, 2009), which receives input from the caudal MDJ. Thus, the two loops, that is, the CC-MDJ-IO loop and the CN-MDJ-IO loop, are connected with each other in a topographically consistent way.

4.3 | Convergence of cerebral and cerebellar input to the MDJ

In addition to elucidating the topography of the CC-MDJ-IO and CN-MDJ-IO loops, we also show here for the first time that these two loops share at least in part the same MDJ neurons; indeed, CC pyramidal cells and contralateral CN projection cells converge upon the same MDJ neurons that project to the IO. This conclusion was based on three lines of evidence. First, our small CTB injections in the MDJ simultaneously provided retrograde labeling of cells in the CC and CN as well as anterograde labeling of axonal fibers in the IO (Figure 4); second, our gene-modified transneuronal rabies approach demonstrated the existence of IO-projecting neurons in the MDJ

that do receive direct input from the CC as well as the existence of IO-projecting neurons in the MDJ that do receive direct input from the CN (Figure 6); and third, our triple-tracing experiments (Figure 7) directly revealed individually retrogradely labeled MDJ neurons that received anterogradely labeled axonal input from both the CC and CN, with separately identifiable markers for both inputs. Thereby, our results in mice expand upon classical tracing studies, in which some of the components of the MDJ trajectories were studied in isolation in monkey, cat, or rat (De Zeeuw & Ruigrok, 1994; De Zeeuw et al., 1998; Leichnetz et al., 1984; Mabuchi & Kusama, 1970; McCrea & Baker, 1985; Nakamura et al., 1983a, 1983b; Saint-Cyr, 1987).

4.4 | Role of MDJ and IO in cerebro-cerebellar communication

Multiple lines of research have implicated involvement of the MDJ in CC- and/or cerebellum-dependent behaviors (Halmagyi et al., 1994; Peschanski & Mantyh, 1983; Shiraishi & Nakao, 1994; Wiest et al., 1996). Previous physiological studies provide evidence for direct activation of the IO or increased complex spike activity of Purkinje cells following electrical stimulation of CC regions in awake or anesthetized animals (Crill, 1970; Kato et al., 1988; Pardoe et al., 2004; Sasaki et al., 1975; Watson et al., 2009). Indeed, the complex spike activity of Purkinje cells in crus I, crus II, and vermal lobule VII can be facilitated by stimulating the prefrontal (Watson et al., 2009), motor (Ackerley et al., 2006), and/or somatosensory cortices (Shimuta et al., 2020), in line with the sources in the CC that provide axonal projections onto the olivary-projecting neurons in the MDJ (see e.g., Figures 2, 6, and 7).

What might be the function of the CC-MDJ-IO loop? The widespread distribution of the IO-projecting neurons in the MDJ determines the diverse functions of this pathway in which it might be involved. Given the role of the olivocerebellar system in oculomotor behavior as well as the anatomical findings provided by our data, we speculate that the MDJ-IO pathway could indeed play, among others, a role in oculomotor control, such as exploring the world and generating expectations based upon these explorations. An example of this is reflected by the fact that the rostral MAO receives input from the nucleus of Darkschewitsch of the MDJ and that the climbing fibers originating from the rostral MAO project to the flocculus to control head movements integrated with compensatory eye movements. Neurons in the interstitial nucleus of Cajal and Darkschewitsch nucleus were anatomically identified as pre-oculomotor neurons (Büttner-Ennever & Büttner, 1978; Labandeira-Garcia et al., 1989) which could diverge the signal to the oculomotor nuclei and the IO, controlling rapid and precise oculomotor movements (Quinet et al., 2020). Additionally, given the direct projection from the oculomotor nuclei to the IO (Figure 1), we speculate that the MDJ could also mediate oculomotor function by sending an efference copy to the cerebellum. The climbing fibers arising from the CC-MDJ-IO loop may provide well-timed, teaching, reward, and/or prediction signals to the Purkinje cells that can be used for complex motor and/

or cognitive learning (Heffley et al., 2018; Kostadinov et al., 2019; Ohmae & Medina, 2015). Indeed, an increase in such teacher signals may be used to enhance acquired motor or cognitive responses that are mediated by downbound modules, whereas a decrease in them may be used to drive learning mediated by upbound modules (De Zeeuw, 2021). The increases in climbing fiber activity and associated complex spike activity in the downbound modules may decrease the simple spike activity of Purkinje cells that can drive, for example, a conditioned, accelerated (Ohmae & Medina, 2015; ten Brinke et al., 2015), or delayed (Chabrol et al., 2019; Gao et al., 2018) motor or cognitive response. Conversely, decreases in climbing fiber activity and associated complex spike activity in the upbound modules can increase the simple spike activity of Purkinje cells that can modulate ongoing motor and/or cortical responses (Romano et al., 2018; Voges et al., 2017). Thus the intrinsic biochemical properties of Purkinje cells in downbound and upbound modules that render the baseline firing frequency of their simple spike responses relatively high and low, respectively, may also well cause them to go down or up during learning (De Zeeuw, 2021). Accordingly, it has been hypothesized that the net-polarity of neurotransmissions downstream of the Purkinje cells in downbound and upbound modules are excitatory and inhibitory, respectively, together facilitating bidirectional control (De Zeeuw, 2021). To what extent the modules of the CC-MDJ-IO loop are implicated in downbound and/or upbound modules remains to be elucidated, but given the mixed upbound-downbound biochemical nature of the D-zones of Purkinje cells in the cerebellar cortex, which receive their climbing fibers from the PO, and the upbound biochemical nature of the C2 zone, which receives its climbing fibers from the rostral MAO, bidirectional control of complex motor responses and/or cognitive responses should indeed be possible (Barmack, 2006; Braak et al., 2003; De Zeeuw, 2021; Fujita et al., 2020; Larson et al., 1969).

The CN-MDJ-IO loop may well support the CC-MDJ-IO loop in serving these timing functions during bidirectional control. Whereas the MDJ provides a robust excitatory input to the electrotonically coupled dendritic spines of the PO and rostral MAO, the CN provides an equally robust inhibitory input to the very same dendritic spines (De Zeeuw et al., 1989, 1998; Ruigrok & Voogd, 1995). This configuration of a combined excitatory and inhibitory input to excitable spines within a glomerulus renders the activation of olivary neurons particularly sensitive to the timing between these two inputs (De Zeeuw et al., 1998; Negrello et al., 2019). Moreover, as we have shown in the current study, the CN apparently also provides a prominent projection to MDJ neurons that is topographically aligned with their input from the CC. Thus, both at the level of cyto-architecture of the olivary neuropil and at the level of the network connectivity of the CN-MDJ-IO and CC-MDJ-IO loops, the climbing fiber system appears well-designed to facilitate precise timing of neuronal activity required for complex functions mediated by cerebro-cerebellar control. It will be interesting to elucidate to what extent processing in the cortico-ponto-cerebellar mossy fiber system lines up with that of the cortico-MDJ-IO-cerebellar climbing fiber system in regulating these functions.

DECLARATION OF TRANSPARENCY

The authors, reviewers and editors affirm that in accordance to the policies set by the *Journal of Neuroscience Research*, this manuscript presents an accurate and transparent account of the study being reported and that all critical details describing the methods and results are present.

ACKNOWLEDGMENTS

The authors thank E.H. Sabel-Goedknecht for providing expert technical assistance and M. Rutteman for managing the animal breeding.

CONFLICT OF INTEREST

The authors declare no competing interests.

AUTHOR CONTRIBUTIONS

Conceptualization, X.W., Z.G., T.R., and C.D.Z.; *Formal Analysis*, X.W. and M.N.; *Data Curation*, X.W., M.N., and T.R.; *Writing – Original Draft*, X.W., T.R., and C.D.Z.; *Writing – Review & Editing*, X.W., Z.G., T.R., and C.D.Z.; *Supervision*, X.W., T.R., and C.D.Z.; *Funding Acquisition*, Z.G. and C.D.Z.

PEER REVIEW

The peer review history for this article is available at <https://publons.com/publon/10.1002/jnr.24993>.

DATA AVAILABILITY STATEMENT

The original data from Allen Mouse Brain are available at <https://mouse.brain-map.org/>. For the detailed information about the injections which are included in this work, please see the file in the repository <https://github.com/XiaoluOne/MDJ>. Other anatomical data are available from the corresponding authors upon reasonable request.

REFERENCES

- Abdelgabar, A. R., Suttrup, J., Broersen, R., Bhandari, R., Picard, S., Keyzers, C., De Zeeuw, C. I., & Gazzola, V. (2019). Action perception recruits the cerebellum and is impaired in patients with spinocerebellar ataxia. *Brain*, *142*, 3791–3805. <https://doi.org/10.1093/brain/awz337>
- Ackerley, R., Pardoe, J., & Apps, R. (2006). A novel site of synaptic relay for climbing fibre pathways relaying signals from the motor cortex to the cerebellar cortical C1 zone. *Journal of Physiology*, *576*, 503–518. <https://doi.org/10.1113/jphysiol.2006.114215>
- Akkal, D., Dum, R. P., & Strick, P. L. (2007). Supplementary motor area and presupplementary motor area: Targets of basal ganglia and cerebellar output. *Journal of Neuroscience*, *27*, 10659–10673. <https://doi.org/10.1523/JNEUROSCI.3134-07.2007>
- Amino, Y., Kyuhou, S., Matsuzaki, R., & Gemba, H. (2001). Cerebello-thalamo-cortical projections to the posterior parietal cortex in the macaque monkey. *Neuroscience Letters*, *309*, 29–32. [https://doi.org/10.1016/S0304-3940\(01\)02018-3](https://doi.org/10.1016/S0304-3940(01)02018-3)
- An, X., Bandler, R., Ongür, D., & Price, J. L. (1998). Prefrontal cortical projections to longitudinal columns in the midbrain periaqueductal gray in macaque monkeys. *Journal of Comparative Neurology*, *401*, 455–479. [https://doi.org/10.1002/\(SICI\)1096-9861\(19981130\)401:4<455:AID-CNE3>3.0.CO;2-6](https://doi.org/10.1002/(SICI)1096-9861(19981130)401:4<455:AID-CNE3>3.0.CO;2-6)
- Angelucci, A., Clascá, F., & Sur, M. (1996). Anterograde axonal tracing with the subunit B of cholera toxin: A highly sensitive immunohistochemical protocol for revealing fine axonal morphology in adult and neonatal brains. *Journal of Neuroscience Methods*, *65*, 101–112. [https://doi.org/10.1016/0165-0270\(95\)00155-7](https://doi.org/10.1016/0165-0270(95)00155-7)
- Aoki, S., Coulon, P., & Ruigrok, T. J. H. (2019). Multizonal cerebellar influence over sensorimotor areas of the rat cerebral cortex. *Cerebral Cortex*, *29*, 598–614. <https://doi.org/10.1093/cercor/bhx343>
- Apps, R., & Hawkes, R. (2009). Cerebellar cortical organization: A one-map hypothesis. *Nature Reviews Neuroscience*, *10*, 670–681. <https://doi.org/10.1038/nrn2698>
- Barmack, N. H. (2006). Inferior olive and oculomotor system. *Progress in Brain Research*, *151*, 269–291.
- Bentivoglio, M., & Kuypers, H. G. (1982). Divergent axon collaterals from rat cerebellar nuclei to diencephalon, mesencephalon, medulla oblongata and cervical cord. A fluorescent double retrograde labeling study. *Experimental Brain Research*, *46*, 339–356. <https://doi.org/10.1007/BF00238629>
- Berkley, K. J., Budell, R. J., Blomqvist, A., & Bull, M. (1986). Output systems of the dorsal column nuclei in the cat. *Brain Research*, *396*, 199–225. [https://doi.org/10.1016/0165-0173\(86\)90012-3](https://doi.org/10.1016/0165-0173(86)90012-3)
- Berkley, K. J., & Worden, I. G. (1978). Projections to the inferior olive of the cat. I. Comparisons of input from the dorsal column nuclei, the lateral cervical nucleus, the spino-olivary pathways, the cerebral cortex and the cerebellum. *Journal of Comparative Neurology*, *180*, 237–251. <https://doi.org/10.1002/cne.901800204>
- Berretta, S., Bosco, G., Giaquinta, G., Smecca, G., & Perciavalle, V. (1993). Cerebellar influences on accessory oculomotor nuclei of the rat: A neuroanatomical, immunohistochemical, and electrophysiological study. *Journal of Comparative Neurology*, *338*, 50–66. <https://doi.org/10.1002/cne.903380105>
- Biswas, M. S., Luo, Y., Sarpong, G. A., & Sugihara, I. (2019). Divergent projections of single pontocerebellar axons to multiple cerebellar lobules in the mouse. *Journal of Comparative Neurology*, *527*, 1966–1985. <https://doi.org/10.1002/cne.24662>
- Braak, H., Rüb, U., & Del Tredici, K. (2003). Involvement of precerebellar nuclei in multiple system atrophy. *Neuropathology and Applied Neurobiology*, *29*, 60–76. <https://doi.org/10.1046/j.1365-2990.2003.00432.x>
- Brissenden, J. A., & Somers, D. C. (2019). Cortico-cerebellar networks for visual attention and working memory. *Current Opinion in Psychology*, *29*, 239–247. <https://doi.org/10.1016/j.copsyc.2019.05.003>
- Brodal, P. (1978). Principles of organization of the monkey corticopontine projection. *Brain Research*, *148*, 214–218. [https://doi.org/10.1016/0006-8993\(78\)90392-X](https://doi.org/10.1016/0006-8993(78)90392-X)
- Brown, J. T., Chan-Palay, V., & Palay, S. L. (1977). A study of afferent input to the inferior olivary complex in the rat by retrograde axonal transport of horseradish peroxidase. *Journal of Comparative Neurology*, *176*, 1–22. <https://doi.org/10.1002/cne.901760102>
- Brown, S. T., & Raman, I. M. (2018). Sensorimotor integration and amplification of reflexive whisking by well-timed spiking in the cerebellar corticonuclear circuit. *Neuron*, *99*, 564–575.e2. <https://doi.org/10.1016/j.neuron.2018.06.028>
- Bull, M. S., Mitchell, S. K., & Berkley, K. J. (1990). Convergent inputs to the inferior olive from the dorsal column nuclei and pretectum in the cat. *Brain Research*, *525*, 1–10. [https://doi.org/10.1016/0006-8993\(90\)91314-7](https://doi.org/10.1016/0006-8993(90)91314-7)
- Burman, K., Darian-Smith, C., & Darian-Smith, I. (2000). Macaque red nucleus: Origins of spinal and olivary projections and terminations of cortical inputs. *Journal of Comparative Neurology*, *423*, 179–196. [https://doi.org/10.1002/1096-9861\(20000724\)423:2<179:AID-CNE1>3.0.CO;2-#](https://doi.org/10.1002/1096-9861(20000724)423:2<179:AID-CNE1>3.0.CO;2-#)
- Büttner-Ennever, J. A., & Büttner, U. (1978). A cell group associated with vertical eye movements in the rostral mesencephalic reticular formation of the monkey. *Brain Research*, *151*, 31–47. [https://doi.org/10.1016/0006-8993\(78\)90948-4](https://doi.org/10.1016/0006-8993(78)90948-4)

- Callaway, E. M., & Luo, L. (2015). Monosynaptic circuit tracing with glycoprotein-deleted rabies viruses. *Journal of Neuroscience*, 35, 8979–8985. <https://doi.org/10.1523/JNEUROSCI.0409-15.2015>
- Carlton, S. M., Leichnetz, G. R., & Mayer, J. D. (1982). Projections from the nucleus parafascicularis prerubralis to medullary raphe nuclei and inferior olive in the rat: A horseradish peroxidase and autoradiography study. *Neuroscience Letters*, 30, 191–197. [https://doi.org/10.1016/0304-3940\(82\)90398-6](https://doi.org/10.1016/0304-3940(82)90398-6)
- Chabrol, F. P., Blot, A., & Mrcsic-Flogel, T. D. (2019). Cerebellar contribution to preparatory activity in motor neocortex. *Neuron*, 103, 506–519.e4. <https://doi.org/10.1016/j.neuron.2019.05.022>
- Coffman, K. A., Dum, R. P., & Strick, P. L. (2011). Cerebellar vermis is a target of projections from the motor areas in the cerebral cortex. *Proceedings of the National Academy of Sciences of the United States of America*, 108, 16068–16073. <https://doi.org/10.1073/pnas.1107904108>
- Condé, F., & Condé, H. (1982). The rubro-olivary tract in the cat, as demonstrated with the method of retrograde transport of horseradish peroxidase. *Neuroscience*, 7, 715–724. [https://doi.org/10.1016/0306-4522\(82\)90076-8](https://doi.org/10.1016/0306-4522(82)90076-8)
- Conte, W. L., Kamishina, H., & Reep, R. L. (2009). Multiple neuroanatomical tract-tracing using fluorescent Alexa Fluor conjugates of cholera toxin subunit B in rats. *Nature Protocols*, 4, 1157–1166. <https://doi.org/10.1038/nprot.2009.93>
- Cornwall, J., & Phillipson, O. T. (1988). Afferent projections to the parafascicular thalamic nucleus of the rat, as shown by the retrograde transport of wheat germ agglutinin. *Brain Research Bulletin*, 20, 139–150. [https://doi.org/10.1016/0361-9230\(88\)90171-2](https://doi.org/10.1016/0361-9230(88)90171-2)
- Crill, W. E. (1970). Unitary multiple-spiked responses in cat inferior olive nucleus. *Journal of Neurophysiology*, 33, 199–209. <https://doi.org/10.1152/jn.1970.33.2.199>
- Crippa, A., Del Vecchio, G., Busti Ceccarelli, S., Nobile, M., Arrigoni, F., & Brambilla, P. (2016). Cortico-cerebellar connectivity in autism spectrum disorder: What do we know so far? *Frontiers in Psychiatry*, 7, 20. <https://doi.org/10.3389/fpsy.2016.00020>
- De Zeeuw, C. I. (2021). Bidirectional learning in upbound and downbound microzones of the cerebellum. *Nature Reviews Neuroscience*, 22, 92–110. <https://doi.org/10.1038/s41583-020-00392-x>
- De Zeeuw, C. I., Holstege, J. C., Ruigrok, T. J., & Voogd, J. (1989). Ultrastructural study of the GABAergic, cerebellar, and mesodiencephalic innervation of the cat medial accessory olive: Anterograde tracing combined with immunocytochemistry. *Journal of Comparative Neurology*, 284, 12–35. <https://doi.org/10.1002/cne.902840103>
- De Zeeuw, C. I., & Ruigrok, T. J. (1994). Olivary projecting neurons in the nucleus of Darkschewitsch in the cat receive excitatory monosynaptic input from the cerebellar nuclei. *Brain Research*, 653, 345–350. [https://doi.org/10.1016/0006-8993\(94\)90411-1](https://doi.org/10.1016/0006-8993(94)90411-1)
- De Zeeuw, C. I., Simpson, J. I., Hoogenraad, C. C., Galjart, N., Koekkoek, S. K., & Ruigrok, T. J. (1998). Microcircuitry and function of the inferior olive. *Trends in Neurosciences*, 21, 391–400. [https://doi.org/10.1016/S0166-2236\(98\)01310-1](https://doi.org/10.1016/S0166-2236(98)01310-1)
- Depping, M. S., Schmitgen, M. M., Kubera, K. M., & Wolf, R. C. (2018). Cerebellar contributions to major depression. *Frontiers in Psychiatry*, 9, 634. <https://doi.org/10.3389/fpsy.2018.00634>
- D'Mello, A. M., & Stoodley, C. J. (2015). Cerebro-cerebellar circuits in autism spectrum disorder. *Frontiers in Neuroscience*, 9, 408. <https://doi.org/10.3389/fnins.2015.00408>
- Fujita, H., Kodama, T., & du Lac, S. (2020). Modular output circuits of the fastigial nucleus for diverse motor and nonmotor functions of the cerebellar vermis. *eLife*, 9, e58613. <https://doi.org/10.7554/eLife.58613>
- Fukushima, K., Terashima, T., Kudo, J., Inoue, Y., & Kato, M. (1986). Projections of the group y of the vestibular nuclei and the dentate and fastigial nuclei of the cerebellum to the interstitial nucleus of Cajal. *Neuroscience Research*, 3, 285–299. [https://doi.org/10.1016/0168-0102\(86\)90021-0](https://doi.org/10.1016/0168-0102(86)90021-0)
- Gao, Z., Davis, C., Thomas, A. M., Economo, M. N., Abrego, A. M., Svoboda, K., De Zeeuw, C. I., & Li, N. (2018). A cortico-cerebellar loop for motor planning. *Nature*, 563, 113–116. <https://doi.org/10.1038/s41586-018-0633-x>
- Glickstein, M., May, J. G., 3rd, & Mercier, B. E. (1985). Corticopontine projection in the macaque: The distribution of labelled cortical cells after large injections of horseradish peroxidase in the pontine nuclei. *Journal of Comparative Neurology*, 235, 343–359. <https://doi.org/10.1002/cne.902350306>
- Gonzalo-Ruiz, A., Leichnetz, G. R., & Hardy, S. G. (1990). Projections of the medial cerebellar nucleus to oculomotor-related midbrain areas in the rat: An anterograde and retrograde HRP study. *Journal of Comparative Neurology*, 296, 427–436. <https://doi.org/10.1002/cne.902960308>
- Gonzalo-Ruiz, A., Leichnetz, G. R., & Smith, D. J. (1988). Origin of cerebellar projections to the region of the oculomotor complex, medial pontine reticular formation, and superior colliculus in new world monkeys: A retrograde horseradish peroxidase study. *Journal of Comparative Neurology*, 268, 508–526. <https://doi.org/10.1002/cne.902680404>
- Guo, J.-Z., Sauerbrei, B., Cohen, J. D., Mischiati, M., Graves, A., Pisanello, F., Branson, K., & Hantman, A. W. (2020). Dynamics of the cortico-cerebellar loop fine-tune dexterous movement. *bioRxiv*, 637447.
- Halmagyi, G. M., Aw, S. T., Dehaene, I., Curthoys, I. S., & Todd, M. J. (1994). Jerk-waveform see-saw nystagmus due to unilateral meso-diencephalic lesion. *Brain*, 117(Pt 4), 789–803. <https://doi.org/10.1093/brain/117.4.789>
- Hamada, M., Strigaro, G., Murase, N., Sadnicka, A., Galea, J. M., Edwards, M. J., & Rothwell, J. C. (2012). Cerebellar modulation of human associative plasticity. *Journal of Physiology*, 590, 2365–2374. <https://doi.org/10.1113/jphysiol.2012.230540>
- Heffley, W., Song, E. Y., Xu, Z., Taylor, B. N., Hughes, M. A., McKinney, A., Joshua, M., & Hull, C. (2018). Coordinated cerebellar climbing fiber activity signals learned sensorimotor predictions. *Nature Neuroscience*, 21, 1431–1441. <https://doi.org/10.1038/s41593-018-0228-8>
- Henschke, J. U., & Pakan, J. M. (2020). Disynaptic cerebrocerebellar pathways originating from multiple functionally distinct cortical areas. *eLife*, 9, e59148. <https://doi.org/10.7554/eLife.59148>
- Hoover, W. B., & Vertes, R. P. (2007). Anatomical analysis of afferent projections to the medial prefrontal cortex in the rat. *Brain Structure and Function*, 212, 149–179. <https://doi.org/10.1007/s00429-007-0150-4>
- Igelström, K. M., Webb, T. W., & Graziano, M. S. A. (2017). Functional connectivity between the temporoparietal cortex and cerebellum in autism spectrum disorder. *Cerebral Cortex*, 27, 2617–2627.
- Kalil, K. (1981). Projections of the cerebellar and dorsal column nuclei upon the thalamus of the rhesus monkey. *Journal of Comparative Neurology*, 195, 25–50. <https://doi.org/10.1002/cne.901950105>
- Kato, N., Kawaguchi, S., & Miyata, H. (1988). Cerebro-cerebellar projections from the lateral suprasylvian visual area in the cat. *Journal of Physiology*, 395, 473–485. <https://doi.org/10.1113/jphysiol.1988.sp016930>
- Kim, E. J., Jacobs, M. W., Ito-Cole, T., & Callaway, E. M. (2016). Improved monosynaptic neural circuit tracing using engineered rabies virus glycoproteins. *Cell Reports*, 15, 692–699. <https://doi.org/10.1016/j.celrep.2016.03.067>
- Kostadinov, D., Beau, M., Blanco-Pozo, M., & Häusser, M. (2019). Predictive and reactive reward signals conveyed by climbing fiber inputs to cerebellar Purkinje cells. *Nature Neuroscience*, 22, 950–962. <https://doi.org/10.1038/s41593-019-0381-8>
- Kubo, R., Aiba, A., & Hashimoto, K. (2018). The anatomical pathway from the mesodiencephalic junction to the inferior olive relays

- perioral sensory signals to the cerebellum in the mouse. *Journal of Physiology*, 596, 3775–3791. <https://doi.org/10.1113/JP275836>
- Labandeira-Garcia, J. L., Guerra-Seijas, M. J., & Labandeira-Garcia, J. A. (1989). Oculomotor nucleus afferents from the interstitial nucleus of Cajal and the region surrounding the fasciculus retroflexus in the rabbit. *Neuroscience Letters*, 101, 11–16. [https://doi.org/10.1016/0304-3940\(89\)90432-1](https://doi.org/10.1016/0304-3940(89)90432-1)
- Larson, B., Miller, S., & Oscarsson, O. (1969). Termination and functional organization of the dorsolateral spino-olivocerebellar path. *Journal of Physiology*, 203, 611–640. <https://doi.org/10.1113/jphysiol.1969.sp008882>
- Leergaard, T. B. (2003). Clustered and laminar topographic patterns in rat cerebro-pontine pathways. *Anatomy and Embryology*, 206, 149–162. <https://doi.org/10.1007/s00429-002-0272-7>
- Leergaard, T. B., Lyngstad, K. A., Thompson, J. H., Taeymans, S., Vos, B. P., De Schutter, E., Bower, J. M., & Bjaalie, J. G. (2000). Rat somatosensory cerebropontocerebellar pathways: Spatial relationships of the somatotopic map of the primary somatosensory cortex are preserved in a three-dimensional clustered pontine map. *Journal of Comparative Neurology*, 422, 246–266. [https://doi.org/10.1002/\(SICI\)1096-9861\(20000626\)422:2<246:AID-CNE7>3.0.CO;2-R](https://doi.org/10.1002/(SICI)1096-9861(20000626)422:2<246:AID-CNE7>3.0.CO;2-R)
- Legg, C. R., Mercier, B., & Glickstein, M. (1989). Corticopontine projection in the rat: The distribution of labelled cortical cells after large injections of horseradish peroxidase in the pontine nuclei. *Journal of Comparative Neurology*, 286, 427–441. <https://doi.org/10.1002/cne.902860403>
- Leichnetz, G. R., Spencer, R. F., & Smith, D. J. (1984). Cortical projections to nuclei adjacent to the oculomotor complex in the medial diencephalic tegmentum in the monkey. *Journal of Comparative Neurology*, 228, 359–387.
- Linauts, M., & Martin, G. F. (1978). An autoradiographic study of midbrain-diencephalic projections to the inferior olivary nucleus in the opossum (*Didelphis virginiana*). *Journal of Comparative Neurology*, 179, 325–353. <https://doi.org/10.1002/cne.901790206>
- Lindeman, S., Hong, S., Kros, L., Mejias, J. F., Romano, V., Oostenveld, R., Negrello, M., Bosman, L. W. J., & De Zeeuw, C. I. (2021). Cerebellar Purkinje cells can differentially modulate coherence between sensory and motor cortex depending on region and behavior. *Proceedings of the National Academy of Sciences of the United States of America*, 118, e2015292118. <https://doi.org/10.1073/pnas.2015292118>
- Mabuchi, M., & Kusama, T. (1970). Mesodiencephalic projections to the inferior olive and the vestibular and perihypoglossal nuclei. *Brain Research*, 17, 133–136. [https://doi.org/10.1016/0006-8993\(70\)90314-8](https://doi.org/10.1016/0006-8993(70)90314-8)
- Mandelbaum, G., Taranda, J., Haynes, T. M., Hochbaum, D. R., Huang, K. W., Hyun, M., Umadevi Venkataraju, K., Straub, C., Wang, W., Robertson, K., Osten, P., & Sabatini, B. L. (2019). Distinct cortical-thalamic-striatal circuits through the parafascicular nucleus. *Neuron*, 102, 636–652.e7. <https://doi.org/10.1016/j.neuron.2019.02.035>
- Massion, J. (1967). The mammalian red nucleus. *Physiological Reviews*, 47, 383–436. <https://doi.org/10.1152/physrev.1967.47.3.383>
- McCrea, R. A., & Baker, R. (1985). Anatomical connections of the nucleus prepositus of the cat. *Journal of Comparative Neurology*, 237, 377–407. <https://doi.org/10.1002/cne.902370308>
- Mitrofanis, J., & deFonseka, R. (2001). Organisation of connections between the zona incerta and the interposed nucleus. *Anatomy and Embryology*, 204, 153–159. <https://doi.org/10.1007/s004290100187>
- Murphy, M. J. M., & Deutch, A. Y. (2018). Organization of afferents to the orbitofrontal cortex in the rat. *Journal of Comparative Neurology*, 526, 1498–1526. <https://doi.org/10.1002/cne.24424>
- Nakamura, Y., Kitao, Y., & Okoyama, S. (1983a). Cortico-Darkschewitsch-olivary projection in the cat: An electron microscope study with the aid of horseradish peroxidase tracing technique. *Brain Research*, 274, 140–143. [https://doi.org/10.1016/0006-8993\(83\)90529-2](https://doi.org/10.1016/0006-8993(83)90529-2)
- Nakamura, Y., Kitao, Y., & Okoyama, S. (1983b). Projections from the pericruciate cortex to the nucleus of Darkschewitsch and other structures at the mesodiencephalic junction in the cat. *Brain Research Bulletin*, 10, 517–521. [https://doi.org/10.1016/0361-9230\(83\)90149-1](https://doi.org/10.1016/0361-9230(83)90149-1)
- Negrello, M., Warnaar, P., Romano, V., Owens, C. B., Lindeman, S., Iavarone, E., Spanke, J. K., Bosman, L. W. J., & De Zeeuw, C. I. (2019). Quasiperiodic rhythms of the inferior olive. *PLoS Computational Biology*, 15, e1006475. <https://doi.org/10.1371/journal.pcbi.1006475>
- Oh, S. W., Harris, J. A., Ng, L., Winslow, B., Cain, N., Mihalas, S., Wang, Q., Lau, C., Kuan, L., Henry, A. M., Mortrud, M. T., Ouellette, B., Nguyen, T. N., Sorensen, S. A., Slaughterbeck, C. R., Wakeman, W., Li, Y., Feng, D., Ho, A., ... Zeng, H. (2014). A mesoscale connectome of the mouse brain. *Nature*, 508, 207–214. <https://doi.org/10.1038/nature13186>
- Ohmae, S., Kunimatsu, J., & Tanaka, M. (2017). Cerebellar roles in self-timing for sub- and supra-second intervals. *Journal of Neuroscience*, 37, 3511–3522. <https://doi.org/10.1523/JNEUROSCI.2221-16.2017>
- Ohmae, S., & Medina, J. F. (2015). Climbing fibers encode a temporal-difference prediction error during cerebellar learning in mice. *Nature Neuroscience*, 18, 1798–1803. <https://doi.org/10.1038/nn.4167>
- Olivito, G., Clausi, S., Laghi, F., Tedesco, A. M., Baiocco, R., Mastropasqua, C., Molinari, M., Cercignani, M., Bozzali, M., & Leggio, M. (2017). Resting-state functional connectivity changes between dentate nucleus and cortical social brain regions in autism spectrum disorders. *Cerebellum*, 16, 283–292. <https://doi.org/10.1007/s12311-016-0795-8>
- Onodera, S. (1984). Olivary projections from the mesodiencephalic structures in the cat studied by means of axonal transport of horseradish peroxidase and tritiated amino acids. *Journal of Comparative Neurology*, 227, 37–49. <https://doi.org/10.1002/cne.902270106>
- Onodera, S., & Hicks, T. P. (1996). A projection linking motor cortex with the LM-supragenulate nuclear complex through the periaqueductal gray area which surrounds the nucleus of Darkschewitsch in the cat. *Progress in Brain Research*, 112, 85–98.
- Onodera, S., & Hicks, T. P. (2009). A comparative neuroanatomical study of the red nucleus of the cat, macaque and human. *PLoS One*, 4, e6623.
- Onuki, Y., Van Someren, E. J., De Zeeuw, C. I., & Van der Werf, Y. D. (2015). Hippocampal-cerebellar interaction during spatio-temporal prediction. *Cerebral Cortex*, 25, 313–321. <https://doi.org/10.1093/cercor/bht221>
- Pardoe, J., Edgley, S. A., Drew, T., & Apps, R. (2004). Changes in excitability of ascending and descending inputs to cerebellar climbing fibers during locomotion. *Journal of Neuroscience*, 24, 2656–2666. <https://doi.org/10.1523/JNEUROSCI.1659-03.2004>
- Paxinos, G., Franklin, K. B., & (2019). , *Paxinos and Franklin's the mouse brain in stereotaxic coordinates*. Academic Press.
- Peschanski, M., & Mantyh, P. W. (1983). Efferent connections of the sub-fascicular area of the mesodiencephalic junction and its possible involvement in stimulation-produced analgesia. *Brain Research*, 263, 181–190. [https://doi.org/10.1016/0006-8993\(83\)90311-6](https://doi.org/10.1016/0006-8993(83)90311-6)
- Popa, T., Velayudhan, B., Hubsch, C., Pradeep, S., Roze, E., Vidailhet, M., Meunier, S., & Kishore, A. (2013). Cerebellar processing of sensory inputs primes motor cortex plasticity. *Cerebral Cortex*, 23, 305–314. <https://doi.org/10.1093/cercor/bhs016>
- Proville, R. D., Spolidoro, M., Guyon, N., Dugué, G. P., Selimi, F., Isope, P., Popa, D., & Léna, C. (2014). Cerebellum involvement in cortical sensorimotor circuits for the control of voluntary movements. *Nature Neuroscience*, 17, 1233–1239. <https://doi.org/10.1038/nn.3773>

- Quartarone, A., Cacciola, A., Milardi, D., Ghilardi, M. F., Calamuneri, A., Chillemi, G., Anastasi, G., & Rothwell, J. (2020). New insights into cortico-basal-cerebellar connectome: Clinical and physiological considerations. *Brain*, *143*, 396–406.
- Quinet, J., Schultz, K., May, P. J., & Gamlin, P. D. (2020). Neural control of rapid binocular eye movements: Saccade-vergence burst neurons. *Proceedings of the National Academy of Sciences of the United States of America*, *117*, 29123–29132. <https://doi.org/10.1073/pnas.2015318117>
- Ramrani, N. (2006). The primate cortico-cerebellar system: Anatomy and function. *Nature Reviews Neuroscience*, *7*, 511–522. <https://doi.org/10.1038/nrn1953>
- Rispaal-Padel, L., & Granger, A. (1977). The cerebello-thalamo-cortical pathway. Topographical investigation at the unitary level in the cat. *Experimental Brain Research*, *28*, 101–123.
- Romano, V., De Propriis, L., Bosman, L. W., Warnaar, P., Ten Brinke, M. M., Lindeman, S., Ju, C., Velauthapillai, A., Spanke, J. K., Middendorp Guerra, E., Hoogland, T. M., Negrello, M., D'Angelo, E., & De Zeeuw, C. I. (2018). Potentiation of cerebellar Purkinje cells facilitates whisker reflex adaptation through increased simple spike activity. *eLife*, *7*, e38852. <https://doi.org/10.7554/eLife.38852>
- Royce, G. J., Bromley, S., & Gracco, C. (1991). Subcortical projections to the centromedian and parafascicular thalamic nuclei in the cat. *Journal of Comparative Neurology*, *306*, 129–155. <https://doi.org/10.1002/cne.903060110>
- Ruigrok, T. J. (2011). Ins and outs of cerebellar modules. *Cerebellum*, *10*, 464–474. <https://doi.org/10.1007/s12311-010-0164-y>
- Ruigrok, T. J., Sillitoe, R. V., & Voogd, J. (2004). Chapter 9 - Cerebellum and cerebellar connections. In G. Paxinos (Ed.), *The rat nervous system* (pp. 167–204). Academic Press.
- Ruigrok, T. J., & Teune, T. M. (2014). Collateralization of cerebellar output to functionally distinct brainstem areas. A retrograde, non-fluorescent tracing study in the rat. *Frontiers in Systems Neuroscience*, *8*:23.
- Ruigrok, T. J., & Voogd, J. (1995). Cerebellar influence on olivary excitability in the cat. *European Journal of Neuroscience*, *7*, 679–693. <https://doi.org/10.1111/j.1460-9568.1995.tb00672.x>
- Ruigrok, T. J., & Voogd, J. (2000). Organization of projections from the inferior olive to the cerebellar nuclei in the rat. *Journal of Comparative Neurology*, *426*, 209–228. [https://doi.org/10.1002/1096-9861\(20001016\)426:2<209:AID-CNE4>3.0.CO;2-0](https://doi.org/10.1002/1096-9861(20001016)426:2<209:AID-CNE4>3.0.CO;2-0)
- Rutherford, J. G., Anderson, W. A., & Gwyn, D. G. (1984). A reevaluation of midbrain and diencephalic projections to the inferior olive in rat with particular reference to the rubro-olivary pathway. *Journal of Comparative Neurology*, *229*, 285–300. <https://doi.org/10.1002/cne.902290213>
- Rutherford, J. G., Zuk-Harper, A., & Gwyn, D. G. (1989). A comparison of the distribution of the cerebellar and cortical connections of the nucleus of Darkschewitsch (ND) in the cat: A study using anterograde and retrograde HRP tracing techniques. *Anatomy and Embryology*, *180*, 485–496. <https://doi.org/10.1007/BF00305124>
- Saint-Cyr, J. A. (1983). The projection from the motor cortex to the inferior olive in the cat. An experimental study using axonal transport techniques. *Neuroscience*, *10*, 667–684. [https://doi.org/10.1016/0306-4522\(83\)90209-9](https://doi.org/10.1016/0306-4522(83)90209-9)
- Saint-Cyr, J. A. (1987). Anatomical organization of cortico-mesencephalo-olivary pathways in the cat as demonstrated by axonal transport techniques. *Journal of Comparative Neurology*, *257*, 39–59. <https://doi.org/10.1002/cne.902570105>
- Saint-Cyr, J. A., & Courville, J. (1981). Sources of descending afferents to the inferior olive from the upper brain stem in the cat as revealed by the retrograde transport of horseradish peroxidase. *Journal of Comparative Neurology*, *198*, 567–581. <https://doi.org/10.1002/cne.901980403>
- Sasaki, K., Oka, H., Matsuda, Y., Shimono, T., & Mizuno, N. (1975). Electrophysiological studies of the projections from the parietal association area to the cerebellar cortex. *Experimental Brain Research*, *23*, 91–102. <https://doi.org/10.1007/BF00238732>
- Shimuta, M., Sugihara, I., & Ishikawa, T. (2020). Multiple signals evoked by unisensory stimulation converge onto cerebellar granule and Purkinje cells in mice. *Communications Biology*, *3*, 381. <https://doi.org/10.1038/s42003-020-1110-2>
- Shinoda, Y., Kakei, S., Futami, T., & Wannier, T. (1993). Thalamocortical organization in the cerebello-thalamo-cortical system. *Cerebral Cortex*, *3*, 421–429. <https://doi.org/10.1093/cercor/3.5.421>
- Shiraishi, Y., & Nakao, S. (1994). Projections of vertical eye movement-related and head rotation-related neurons in the medial mesodiencephalic junction to pontine reticular formation in cat. *Neuroscience Letters*, *171*, 85–88. [https://doi.org/10.1016/0304-3940\(94\)90611-4](https://doi.org/10.1016/0304-3940(94)90611-4)
- Stanton, G. B. (1980). Topographical organization of ascending cerebellar projections from the dentate and interposed nuclei in Macaca mulatta: An anterograde degeneration study. *Journal of Comparative Neurology*, *190*, 699–731. <https://doi.org/10.1002/cne.901900406>
- Strominger, N. L., Truscott, T. C., Miller, R. A., & Royce, G. J. (1979). An autoradiographic study of the rubroolivary tract in the rhesus monkey. *Journal of Comparative Neurology*, *183*, 33–45. <https://doi.org/10.1002/cne.901830104>
- Suzuki, L., Coulon, P., Sabel-Goedknecht, E. H., & Ruigrok, T. J. (2012). Organization of cerebral projections to identified cerebellar zones in the posterior cerebellum of the rat. *Journal of Neuroscience*, *32*, 10854–10869. <https://doi.org/10.1523/JNEUROSCI.0857-12.2012>
- Swenson, R. S., & Castro, A. J. (1983). The afferent connections of the inferior olivary complex in rats. An anterograde study using autoradiographic and axonal degeneration techniques. *Neuroscience*, *8*, 259–275.
- ten Brinke, M. M., Boele, H.-J., Spanke, J. K., Potters, J.-W., Kornysheva, K., Wulff, P., Ijpeelaar, A. C. H. G., Koekkoek, S. K. E., & De Zeeuw, C. I. (2015). Evolving models of Pavlovian conditioning: Cerebellar cortical dynamics in awake behaving mice. *Cell Reports*, *13*, 1977–1988. <https://doi.org/10.1016/j.celrep.2015.10.057>
- Teune, T. M., van der Burg, J., van der Moer, J., Voogd, J., & Ruigrok, T. J. (2000). Topography of cerebellar nuclear projections to the brain stem in the rat. *Progress in Brain Research*, *124*, 141–172.
- Voges, K., Wu, B., Post, L., Schonewille, M., & De Zeeuw, C. I. (2017). Mechanisms underlying vestibulo-cerebellar motor learning in mice depend on movement direction. *Journal of Physiology*, *595*, 5301–5326. <https://doi.org/10.1113/JP274346>
- Voogd, J., & Ruigrok, T. J. (2004). The organization of the corticonuclear and olivocerebellar climbing fiber projections to the rat cerebellar vermis: The congruence of projection zones and the zebrin pattern. *Journal of Neurocytology*, *33*, 5–21. <https://doi.org/10.1023/B:NEUR.0000029645.72074.2b>
- Wagner, M. J., Kim, T. H., Kadmon, J., Nguyen, N. D., Ganguli, S., Schnitzer, M. J., & Luo, L. (2019). Shared cortex-cerebellum dynamics in the execution and learning of a motor task. *Cell*, *177*, 669–682. <https://doi.org/10.1016/j.cell.2019.02.019>
- Walberg, F., & Nordby, T. (1981). A re-examination of the rubro-olivary tract in the cat, using horseradish peroxidase as a retrograde and an anterograde neuronal tracer. *Neuroscience*, *6*, 2379–2391. [https://doi.org/10.1016/0306-4522\(81\)90024-5](https://doi.org/10.1016/0306-4522(81)90024-5)
- Wall, N. R., Wickersham, I. R., Cetin, A., De La Parra, M., & Callaway, E. M. (2010). Monosynaptic circuit tracing in vivo through Cre-dependent targeting and complementation of modified rabies virus. *Proceedings of the National Academy of Sciences of the United States of America*, *107*, 21848–21853. <https://doi.org/10.1073/pnas.1011756107>
- Watson, T., Jones, M., & Apps, R. (2009). Electrophysiological mapping of novel prefrontal–Cerebellar pathways. *Frontiers in Integrative Neuroscience*, *3*, 18. <https://doi.org/10.3389/neuro.07.018.2009>
- Wiesendanger, R., & Wiesendanger, M. (1982). The corticopontine system in the rat. II. The projection pattern. *Journal of Comparative Neurology*, *208*, 227–238. <https://doi.org/10.1002/cne.902080303>

Wiest, G., Baumgartner, C., Schnider, P., Trattig, S., Deecke, L., & Mueller, C. (1996). Monocular elevation paresis and contralateral downgaze paresis from unilateral mesodiencephalic infarction. *Journal of Neurology, Neurosurgery and Psychiatry*, *60*, 579–581. <https://doi.org/10.1136/jnnp.60.5.579>

SUPPORTING INFORMATION

Additional supporting information may be found in the online version of the article at the publisher's website.

Table S1. Stereotaxic coordinates of nuclei

Figure S1. Architecture of the MDJ nuclei projecting to the IO. Areas on the left and right side represent the more rostral and caudal subregions of the MDJ, respectively. Dk, nucleus of Darkschewitsch; FR, fasciculus retroflexus; InC, interstitial nucleus of Cajal; MA3, medial accessory oculomotor nucleus; NB, medial accessory nucleus of Bechterew; PR, prerubral field; RI, rostral interstitial nucleus of the medial longitudinal fasciculus

Figure S2. Individual CTB injections in the IO and retrograde labelling in the MDJ. Seven mice were injected with CTB in different subnuclei of the IO providing different sets of retrogradely labelled neurons in the MDJ at the various rostrocaudal levels. The injections are ordered according to their densities in the MDJ with the most prominent labelling in the rostral and caudal subregions at the top and bottom, respectively. Likewise, the MDJ subregions in the right column are ordered according to the rostrocaudal level of their core part. See abbreviations in Figure S1

Figure S3. Retrogradely labelled cells in the MDJ following CTB injection in the medullary reticular formation (MdV). (a) Coronal section of the injection site from an example mouse. (b) Serial sections of anteroposterior MDJ regions, showing sparse retrograde labelling in the ipsilateral MDJ (insets)

Figure S4. Summary of CTB tracing experiments. In addition to the two representative cases that are shown in Figures 3–5, we here

show the results of seven other animals. From left to right: side view of three-dimensional reconstruction of injection sites (for color codes see Figure 3), retrograde labelling in flattened maps of the cerebral cortical (CC), retrograde labelling in flattened maps of the cerebellar nuclei (CN), and anterograde labelling in flattened maps of the subnuclei of the inferior olive (IO)

Figure S5. Input and output maps of the PAG. (a and b) Coronal sections showing CTB injection in the PAG (a) with sparsely labelled axons in the IO (b). (c and d) Retrogradely labelled cells in the CC and the CN. Upper panels: representative sections showing densely CTB-labelled pyramidal cells in the ipsilateral prefrontal cortical regions and relatively few labelled cells in the contralateral CN. Lower panels: series of rostrocaudal plots of the labelled cells in CC and CN. (e) Summary of injection site as well as input and output maps of PAG. Top panel shows the three-dimensional reconstruction of the injection site. In red: CTB injection site, blue: midbrain contour, grey: third ventricle, green: FR. For abbreviations, see Figure 2

Video S1. Reconstruction of the CTB-labelled cells in the midbrain regions. Reconstruction was made from a representative mouse as in Figure 1. Structures in colors, blue: cerebral peduncle; dark yellow: substantia nigra; green: fasciculus retroflexus; gray: aqueduct; light pink: red nuclei. Colors for labeling, red: MDJ labeling; grey: other labelled cells in the midbrain

Transparent Science Questionnaire for Authors

How to cite this article: Wang, X., Novello, M., Gao, Z., Ruigrok, T. J. H., & De Zeeuw, C. I. (2022). Input and output organization of the mesodiencephalic junction for cerebro-cerebellar communication. *Journal of Neuroscience Research*, *100*, 620–637. <https://doi.org/10.1002/jnr.24993>